

NONSTRUCTURAL COMPONENTS IN CONTROLLED ROCKING BRACED
FRAMES

NONSTRUCTURAL COMPONENT DEMANDS IN BUILDINGS WITH
CONTROLLED ROCKING STEEL BRACED FRAMES

BY NATHAN BUCCELLA, B.Eng.Mgmt.

A Thesis Submitted to the School of Graduate Studies in Partial Fulfilment of the
Requirements for the Degree of Master of Applied Science

Master of Applied Science (2019)
(Civil Engineering)

McMaster University
Hamilton, Ontario, Canada

TITLE: Nonstructural Component Demands in Buildings with
 Controlled Rocking Steel Braced Frames

AUTHOR: Nathan Buccella

SUPERVISORS: Dr. Lydell Andree Wiebe, Dr. Dimitrios Konstantinidis

PAGES: 111 pages (xiv, 97)

Lay Abstract

Controlled Rocking Steel Braced Frames (CRSBFs) have been proposed as a high-performance structural system that resists earthquake forces on buildings. This system has the ability to minimize damage to structural members and self-centre the building back to its original position after an earthquake, two characteristics that are typically not achieved by current conventional systems. However, an assessment of the CRSBF's overall effectiveness cannot be limited to the consideration of only the structural skeleton, as the performance of nonstructural components (e.g. architectural elements, mechanical and electrical equipment, furnishings, and building contents) that are not part of the structural skeleton can have a significant impact on the safety and economic performance of earthquake resisting systems.

This thesis compares the demands on nonstructural components in buildings with CRSBFs to their demands in a more conventional system during earthquake motions. The results show that the trade-off for avoiding damage to structural members in the CRSBFs is often higher demands on the nonstructural components.

Abstract

Controlled Rocking Steel Braced Frames (CRSBFs) have been developed as a high-performance structural solution to resist seismic forces, due to their ability to minimize structural damage and self-centre the structure back to its original position after an earthquake. A CRSBF is intentionally allowed to uplift and rock on its foundation, which acts as the nonlinear mechanism for the system rather than member yielding and buckling. While the CRSBF is in the rocking phase, the response of the system is controlled by prestressing which anchors the frame to the foundation and energy dissipation devices which are engaged by uplift. Although CRSBFs have shown promising structural performance, an assessment of the overall effectiveness of this system must also consider the performance of nonstructural components which have a significant impact on the safety and economic performance of the system.

The purpose of this thesis is to compare the performance of nonstructural components in buildings with CRSBFs to their performance in a conventional codified system such as a buckling restrained braced frame (BRBF), while also investigating which design parameters influence nonstructural component demands in CRSBFs. The responses of various types of nonstructural components, including anchored components, stocky unanchored components that slide, and slender unanchored components that rock, are determined using a cascading analysis approach where absolute floor accelerations generated from nonlinear time-history analyses of each structural system are used as input for computing the responses of nonstructural components. The results show that the trade-off of maintaining elastic behaviour of the CRSBF members is, in general, larger demands on nonstructural components compared to the BRBF system. The results also show that the stiffness of the frame and vibration of the frame in its elastic higher modes are the main influencers for nonstructural component demands in buildings with CRSBFs, while energy dissipation has a minimal impact.

Acknowledgements

I truly feel blessed by the amount of support that I have received from so many people in the completion of this thesis.

I would first like to thank both of my supervisors, Lydell Wiebe and Dimitrios Konstantinidis. Thank you to Lydell for encouraging me to challenge my own observations and dig deeper into solving the questions at hand, and to Dimitri for reminding me to investigate and understand the fundamentals of each problem before diving into the bigger picture. The genuine effort and passion that both Lydell and Dimitri put into teaching their students does not go without notice. I would also like to thank Taylor Steele for sharing his models with me and providing valuable technical support, especially during busy times.

I am also thankful for my friends and colleagues at McMaster who have made my graduate studies so much more than an academic endeavour. The high standard they set for themselves was a constant source of motivation during class work and in the completion of this thesis. Even more so, I am grateful for the countless laughs and comradery that this group of people provided me with.

The work done in this thesis is a direct result of the lifelong support and love provided to me by my parents, Joe and Marie, my sister Savannah, and all of my extended family, and family friends (a list that is exceedingly long and could not be squeezed into this paragraph). I could write an entire thesis on the impact that these people have had on my life and I want them to know that any work that I have produced from the point that I started kindergarten to the culmination of this thesis is a reflection of their support.

Finally, I would like to thank my girlfriend, Rachael Mauro, who was my biggest fan when I needed support, was my best friend when I needed to unwind, and exercised patience when I became wiry. Whenever I became overwhelmed in my work, seeing her at the end of the week was always my main source of motivation.

Table of Contents

Lay Abstract.....	iii
Abstract.....	iv
Acknowledgements.....	v
Table of Contents.....	vi
List of Figures.....	viii
List of Tables.....	x
List of Abbreviations.....	xi
List of Symbols.....	xii
Declaration of Academic Achievement.....	xiv
Chapter: 1 Introduction.....	1
1.1 Background: The CRSBF System.....	1
1.1.1 Higher-Mode Effects.....	3
1.1.2 Abrupt Stiffness Changes.....	4
1.1.3 Previous Studies on Nonstructural Component Demands in CRSBFs.....	5
1.2 Background: Nonstructural Components.....	6
1.3 Objectives.....	8
Chapter: 2 Design of Seismic Force Resisting Systems.....	10
2.1 Design of CRSBFs Part I: Base Rocking Joint Design.....	11
2.2 Design of CRSBFs Part II: Capacity Design of Frame Members.....	15
2.3 Design of BRBFs.....	17
2.4 Design Iteration Based on Nonlinear Time-History Analysis.....	20
2.5 Final Design Parameters.....	21
Chapter: 3 Modeling of Seismic Force Resisting Systems.....	26
3.1 CRSBF Model.....	26
3.2 BRBF Model.....	28
Chapter: 4 Ground Motion Selection and Scaling.....	31
Chapter: 5 Nonlinear Time-History Analysis Structural Results.....	33
Chapter: 6 Performance of Nonstructural Components.....	38
6.1 Overview of Nonstructural Component Analysis Procedure.....	38

6.2	Acceleration-Sensitive Anchored Components	41
6.2.1	Rigid Acceleration-Sensitive Anchored Components	41
6.2.2	Non-Rigid Acceleration-Sensitive Anchored Components	44
6.2.3	Comparison of Floor Spectra in Different CRSBF Designs	52
6.3	Unanchored Sliding Components.....	56
6.4	Unanchored Rocking Components.....	66
6.5	Effect of CRSBF Grounding on Nonstructural Component Performance	74
Chapter: 7	Conclusions and Recommendations	78
7.1	Conclusions	78
7.2	Recommendations	83
References	86
Appendix A:	Final Design Frame Sections.....	91
Appendix B:	Floor Spectra with Extended Period Range.....	94
Appendix C:	CRSBF Floor Spectra with Identical Frames and Extended Period Range ..	96

List of Figures

Figure 1.1 CRSBF Hysteretic Response [after Steele and Wiebe, 2016].....	3
Figure 2.1 (a) DBE elastic response spectrum at 5% damping, and (b) 3-storey structural floor plan.....	11
Figure 2.2 Capacity design: a) elastic model of CRSBF rocking about its toe for modal analysis, b) DBE response spectrum and truncated spectrum amplified for higher modes [after Steele and Wiebe, 2016].....	16
Figure 3.1 OpenSees model schematics: (a) CRSBF [after Steele and Wiebe, 2016], (b) BRBF	27
Figure 3.2 Calibration of BRB Brace Hysteresis in OpenSees comparing the equivalent truss element to parallelized beam-column elements	29
Figure 4.1 3-Storey DBE response spectrum and scaled ground motions.....	32
Figure 5.1 3-storey CRSBF and BRBF nonlinear time-history analysis structural results	33
Figure 5.2 6-storey CRSBF and BRBF nonlinear time-history analysis structural results	33
Figure 5.3 12-storey CRSBF and BRBF nonlinear time-history analysis structural results	34
Figure 6.1 Idealized anchored and unanchored nonstructural components	39
Figure 6.2 CRSBF and BRBF median peak floor accelerations at DBE, 1/2 DBE and 1/4 DBE.....	43
Figure 6.3 3-storey CRSBF and BRBF median pseudo-acceleration floor spectra with $\zeta = 2\%$	45
Figure 6.4 6-storey CRSBF and BRBF median pseudo-acceleration floor spectra with $\zeta = 2\%$	49
Figure 6.5 12-storey CRSBF and BRBF median pseudo-acceleration floor spectra with $\zeta = 2\%$	50
Figure 6.6 3-storey CRSBFs designed with identical frames, median pseudo-acceleration floor spectra with $\zeta = 2\%$	54
Figure 6.7 6-storey CRSBFs designed with identical frames, median pseudo-acceleration floor spectra with $\zeta = 2\%$	55
Figure 6.8 12-storey CRSBFs designed with identical frames, median pseudo-acceleration floor spectra with $\zeta = 2\%$	56
Figure 6.9 3-storey CRSBF and BRBF sliding component median displacement spectra	57
Figure 6.10 3-storey CRSBF and BRBF sliding component median velocity spectra.....	57
Figure 6.11 6-storey CRSBF and BRBF sliding component median displacement spectra	59
Figure 6.12 6-storey CRSBF and BRBF sliding component median velocity spectra.....	60
Figure 6.13 12-storey CRSBF and BRBF sliding component median displacement spectra	63
Figure 6.14 12-storey CRSBF and BRBF sliding component median velocity spectra.....	64

Figure 6.15 3-Storey CRSBF and BRBF rocking component median rocking rotation spectra	66
Figure 6.16 6-storey CRSBF and BRBF rocking component median rocking rotation spectra	68
Figure 6.17 12-storey CRSBF and BRBF rocking component median rocking rotation spectra	71
Figure 6.18 3-storey $\beta=25\%$ CRSBF column uplift, floor acceleration, attached component, sliding component and rocking component time-history responses during the Superstition Hills, Poe Road ground motion.....	76
Figure B.1 3-storey CRSBF and BRBF median pseudo-acceleration floor spectra with $\zeta=2\%$ and extended period range	94
Figure B.2 6-storey CRSBF and BRBF median pseudo-acceleration floor spectra with $\zeta=2\%$ and extended period range	94
Figure B.3 12-storey CRSBF and BRBF median pseudo-acceleration floor spectra with $\zeta=2\%$ and extended period range	95
Figure C.1 3-storey CRSBFs designed with identical frames, median pseudo-acceleration floor spectra with $\zeta = 2\%$ with extended period range	96
Figure C.2 6-storey CRSBFs designed with identical frames, median pseudo-acceleration floor spectra with $\zeta = 2\%$ with extended period range	96
Figure C.3 12-storey CRSBFs designed with identical frames, median pseudo-acceleration floor spectra with $\zeta = 2\%$ with extended period range	97

List of Tables

Table 2.1 Final CRSBF structural design parameters.....	21
Table 2.2 Final BRBF design parameters	21
Table 6.1 Average median PFA, and pseudo-acceleration at higher-mode rocking periods of CRSBFs, over all floors above ground level	44
Table A.1 3S- β 25 CRSBF frame members.....	91
Table A.2 3S- β 90 CRSBF frame members.....	91
Table A.3 3S BRBF frame members	91
Table A.4 6S- β 25 CRSBF frame members.....	91
Table A.5 6S- β 90 CRSBF frame members.....	91
Table A.6 6S BRBF frame members	92
Table A.7 12S- β 25 CRSBF frame members.....	92
Table A.8 12S- β 90 CRSBF frame members.....	92
Table A.9 12S BRBF frame members	93

List of Abbreviations

AISC	American Institute of Steel Construction
ASCE	American Society of Civil Engineers
ATC	Applied Technology Council
BRB	Buckling Restrained Brace
BRBF	Buckling Restrained Braced Frame
CRSBF	Controlled Rocking Steel Braced Frame
DBE	Design Basis Earthquake
FEMA	Federal Emergency Management Agency
MCE _R	Maximum Considered Earthquake
ODE	Ordinary Differential Equation
PFA	Peak Floor Acceleration
SDOF	Single-Degree-of-Freedom
2D	Two-Dimensional

List of Symbols

A_{core}	cross-sectional area of BRB core
A_{PT}	cross-sectional area of prestressing
$C_{probable}$	probable BRB compressive force
d_{ED}	moment arm of the energy dissipation device to the rocking toe
d_{PT}	moment arm of the prestressing to the rocking toe
d_W	moment arm of the self-weight of the CRSBF members to the rocking toe
e	coefficient of restitution
E_{PT}	Young's modulus of prestressing tendons
ED	activation force of the friction energy dissipation device
ED_{max}	maximum expected force in the energy dissipation device
F_a	short-period site coefficient
F_v	long-period site coefficient
g	acceleration due to gravity
H_e	effective height of the CRSBF idealized as an SDOF
H_W	combined vertical centre of mass of the floor diaphragm
L_{PT}	length of prestressing
$M_{b,max}$	maximum base rocking joint moment resistance at θ_{max}
$M_{b,min}$	base overturning moment due to the code reduced lateral forces
$M_{b,rock}$	base rocking moment
M_e	effective mass of the CRSBF idealized as an SDOF
M_{ED}	base overturning moment resistance provided by energy dissipation device
M_{PT}	base overturning moment resistance provided by prestressing
M_W	base overturning moment resistance provided by self-weight of the CRSBF members
$PT_{initial}$	initial prestressing force
$PT_{\theta_{max}}$	force in the prestressing at the max allowable base rocking joint rotation
R	force reduction factor
R_{block}	distance from corner to centre of rocking block
$sgn()$	signum function
S_S	short-period MCE_R spectral acceleration
S_1	1-s MCE_R spectral acceleration
T_L	long-period transition period
T_n	natural period, or natural fundamental period of nonstructural components
$T_{probable}$	probable BRB tensile force
u	displacement of sliding block relative to the floor
$\ddot{u}_{floor,x}$	absolute horizontal floor acceleration
W_{self}	combined self-weight of the CRSBF members

W_{trib}	seismic weight tributary to the CRSBF
α	slenderness angle of rocking block
$\overline{\alpha k}$	normalized secondary stiffness of base rocking joint
β	energy dissipation ratio
β_{comp}	compressive strength adjustment factor
γ_{HM}	higher-mode factor for capacity design
ε	axial strain
ζ	viscous damping ratio
η	prestressing ratio
θ	rotation of rocking block
θ_{max}	maximum expected drift
μ	Coulomb friction coefficient
σ_{ysc}	yield stress of BRB core
ω	strain hardening adjustment factor
Ω	overstrength factor of the CRSBF

Declaration of Academic Achievement

The controlled rocking steel braced frame OpenSees model, capacity design procedure MATLAB script, and elastic model of the controlled rocking steel braced frame during the rocking phase for use during capacity design, used in this thesis were developed by Dr. Taylor Steele, who at the time was a Ph.D. candidate with Dr. Wiebe. All other OpenSees models, MATLAB scripts, and Excel Spreadsheets used in the design and numerical modeling discussed herein were developed by Nathan Buccella. Each draft of the thesis, including all figures and tables, were produced by Nathan Buccella, who also subsequently made revisions based on the comments and suggested edits from Dr. Wiebe and Dr. Konstantinidis.

Chapter: 1 Introduction

1.1 Background: The CRSBF System

Controlled rocking steel braced frames (CRSBFs) are self-centring seismic force resisting systems that have been developed as a high-performance structural solution to meeting seismic demands due to their ability to minimize structural damage and residual drifts. These two characteristics represent distinct advantages over current conventional codified seismic force resisting systems, which rely on plastic deformations in structural members and the overall ductility of the system in order to resist earthquake loads. Permanent damage to structural members can require costly repairs to the structure, and residual drifts can also have a significant impact on the loss estimation and rehabilitation of a structure following an earthquake, as it has been suggested that it may become more feasible economically to completely demolish and rebuild structures with residual drifts as low as 0.5% [McCormick *et al.*; 2008]. Although CRSBFs have shown promise as a high-performance system, structural performance is not the only consideration in the overall assessment of the effectiveness of a seismic force resisting system. One area of research that has gained increased attention is the seismic response of nonstructural components, as demands on these components have been shown to have a significant impact on the overall safety and economic performance of buildings. Therefore, in order to evaluate the true seismic resiliency of buildings featuring the CRSBF system, a structure's ability to maintain occupant safety while also minimizing economic losses and recovery time, the performance of nonstructural components must also be assessed.

Extensive research has shown that CRSBFs have the ability to meet seismic demands at and above a design level earthquake while maintaining their self-centring capabilities [Eatherton and Hajjar, 2010; Ma *et al.*, 2010; Roke *et al.*, 2010]. CRSBFs replace the braced bays of a conventional braced frame system with a frame that lies within the gravity framing and is intentionally allowed to uplift and rock about each of its toes, as shown in Figure 1.1. While the frame remains grounded, CRSBFs resist lateral forces in a similar manner to conventional braced frames. However, once the lateral seismic forces exceed the linear elastic range of the system, the frame begins to uplift and rock. This uplifting action acts as the nonlinear mechanism for the CRSBF rather than the member yielding and buckling experienced in a conventional braced frame. Figure 1.1 displays the typical flag-shaped hysteretic response of a CRSBF. The base rocking moment, $M_{b,rock}$, corresponds to the minimum base overturning moment that causes the designed base rocking joint to uplift. Once uplift occurs, resistance to the system overturning is provided by the self-weight of the frame members and a prestressing cable that anchors the frame to the foundation. Although CRSBFs have the potential to carry the tributary gravity loads from the floor diaphragms [e.g. Gledhill *et al.*, 2008; Mottier *et al.*, 2018], the CRSBFs analyzed in this study were assumed to be decoupled from the gravity loads of the floor diaphragms, and thus not carry their loads. This is achievable through a connection between the floor diaphragm and CRSBF that is designed to only transfer the lateral seismic inertial loads [Latham *et al.*, 2013; Steele, 2019]. Additionally, supplemental energy dissipation can be provided by a variety of energy dissipation devices implemented at the column bases that are engaged by uplift. The result is a system where nearly zero residual drifts occur due to

the self-centring capability of the system, uplift relieves the frame members of large seismic demands (allowing them to be designed as capacity protected elements), and energy dissipation devices that have experienced permanent damage can be easily replaced.

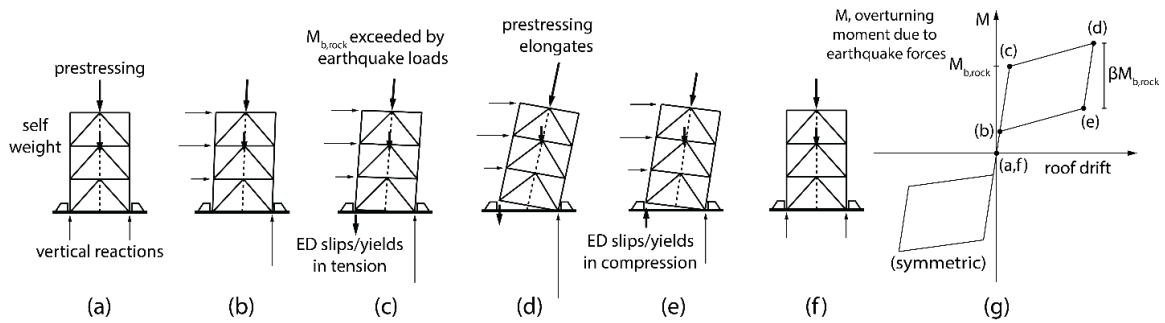


Figure 1.1 CRSBF Hysteretic Response [after Steele and Wiebe, 2016]

1.1.1 Higher-Mode Effects

Although the uplifting mechanism and flag-shaped hysteretic response of CRSBFs provide distinct structural advantages, the demands on nonstructural components in buildings with CRSBFs cannot be assumed to be similar to those experienced in a conventional braced frame seismic force resisting system with distributed plasticity. In past research, nonlinear time-history analyses and shake table testing have shown that CRSBFs can experience a significant increase in frame member forces (in comparison to the expected forces calculated by a modal analysis of the frame using a design level spectral acceleration spectrum reduced by the overall force reduction factor, R , of the system) contributed by the frame vibrating in its higher modes during the rocking phase of the response [Eatherton and Hajjar, 2010; Ma *et al.*, 2010; Roke, 2010; Wiebe *et al.*, 2013]. As an example of the increase in member forces due to higher mode effects, Roke [2010] proposed a modified modal analysis capacity design procedure to ensure that frame members would remain elastic for almost all cases in a numerical study, whereby the modal contribution of the

first-mode lateral forces, at a magnitude that would cause the prestressing to yield, was amplified by a factor of 1.15, and the modal contributions of the second and third modes were amplified by a factor of 2. Therefore, one concern for nonstructural component performance in CRSBFs is whether these higher-mode forces will also translate to increased acceleration demands on nonstructural components.

1.1.2 Abrupt Stiffness Changes

Another concern for nonstructural components in CRSBFs is potential spikes in floor acceleration or nonstructural component demand caused at column impact during rocking [Wiebe and Christopoulos, 2010; Lin *et al.*, 2012]. As previously mentioned, the CRSBFs analyzed in this study were assumed to be decoupled from carrying the gravity loads of the floor diaphragms. Nevertheless, even though vertical spikes in floor acceleration at column impact are not expected for this type of decoupled CRSBF system, there is still concern for lateral floor acceleration spikes. CRSBFs exhibit the behaviour of “clickety-clack” systems [Buchanan *et al.*, 2011], where the overall lateral stiffness of the system transfers from a low-stiffness experienced during the rocking phase, to a high-stiffness experienced at column impact when the frame becomes grounded with the foundation, while occurring at a high velocity. In one study, Lin *et al.* [2012] described multiple sources of anecdotal evidence from the February 22nd, 2011 Christchurch earthquake that suggested building systems exhibiting this type of pinched hysteretic response, such as concrete shear walls, threw building occupants and contents across rooms. Therefore, there may be some concern for spikes in floor accelerations, the accelerations of anchored components and the response of unanchored nonstructural components during grounding of the CRSBF. However, shake

table testing did not show any notable spikes in CRSBF lateral acceleration in a study by Wiebe *et al.* [2013]. Furthermore, although Lin *et al.* [2012] showed that the demands on sliding contents in systems with similar backbone hysteresees were not driven by the change from low to high stiffness but rather the velocity at incipient sliding, the models of the structures captured in this numerical analysis were limited to a single-degree-of-freedom (SDOF).

1.1.3 Previous Studies on Nonstructural Component Demands in CRSBFs

Dyanati *et al.* [2014] compared the structural and nonstructural component performance of a 6-storey CRSBF with those of a conventional concentrically braced frame by performing nonlinear time-history analyses on the two systems in order to build probabilistic demand models for interstorey drifts and peak floor/roof accelerations. They developed fragility curves for the two systems and for four specific nonstructural components that showed that although the self-centring frame experienced better structural and displacement-sensitive component performance than the concentrically braced frame, the demands on acceleration-sensitive components were larger. Although the study provided an indication of the trade-offs between the two systems, the performance of displacement-sensitive components was dependent on design decisions which could vary widely, and the assessment of acceleration-sensitive components was based on peak floor accelerations rather than full floor spectra. A study by Pollino [2014] compared a 3-storey CRSBF to a buckling restrained braced frame (BRBF) structure and showed that the peak magnitudes of the floor spectra in the CRSBF were similar to those in the BRBF. The study also suggested that the floor spectra demands in CRSBFs could be reduced by increasing the

frame rigidity, thereby moving the higher-mode natural periods of the CRSBF outside the range of frequencies of high-energy content in the ground motions, or by allowing for plastic deformation of the frame members. However, the study was limited to a 3-storey structure, and both approaches to reduce the floor spectra tend to work against the main structural advantages of using a CRSBF. Although both studies provided good indications on the performance of nonstructural components in CRSBFs, limitations on the chosen design parameters of the CRSBFs, the number of storeys in each structure and the assessment of other types of nonstructural components, for instance those that are unanchored, represent an area of research that should be addressed in order to provide a well-rounded understanding on the performance of nonstructural components in CRSBFs.

1.2 Background: Nonstructural Components

In the push towards seismic resiliency, the performance of nonstructural components has become a critical aspect of evaluating the effectiveness of various seismic force resisting systems. While ensuring the life safety of building occupants, through collapse prevention, has always been the primary goal of seismic design, large demands on nonstructural components can also pose significant safety risks to building occupants, caused by damage to life-safety systems such as fire suppression piping and hospital equipment, or by large displacements, impacts, and overturning of nonstructural components such as ceiling systems or cladding [ATC, 2012; Comerio, 2005]. The performance of nonstructural components can also have significant economic consequences following an earthquake as these components typically account for up to 80-90% of the total value of a building [Taghavi and Miranda, 2003]. Reconnaissance efforts following past earthquakes, such as

the February 28, 2001 Nisqually earthquake [Filiatrault *et al.*, 2001] and February 27, 2010 Chile earthquake [Miranda *et al.*, 2012], showed that the performance of nonstructural components led to a significant portion of economic losses and downtime following the events.

Because nonstructural components can vary by a wide range of sizes, masses, aspect ratios, and connectivity to the structure, they can also exhibit a wide range of responses, such as vibrating, sliding, rocking, twisting, bouncing, overturning, or other combinations of these motions. Therefore, nonstructural components can be separated into two main categories: anchored and unanchored components. Anchored components are those that are in some way fixed to the structure and can generally be broken down into displacement-sensitive components, such as gypsum board walls or cladding, and acceleration-sensitive components, such as heating and ventilation chiller units or computer equipment such as server cabinets.

Also important is the performance of unanchored components that tend to exhibit large rigid-body motion. This study focuses on the responses of unanchored components that sit on the floor and are free to either slide or rock. Although a combination of these two response modes is also possible, for simplicity and ease of comparison of nonstructural component demands between structural systems in this study, components with a pure sliding or pure rocking response were analyzed separately. The seismic response of sliding components that are both unanchored and stocky enough to slide freely relative to the floor has been studied by a number of researchers in the past [Shao and Tung, 1999; Choi and Tung, 2002; Lopez Garcia and Soong, 2003a; Chaudhuri and Hutchinson, 2005;

Hutchinson and Chaudhuri, 2006; Konstantinidis and Makris, 2009, 2010; Lin *et al.*, 2015; Nikfar and Konstantinidis, 2017; Van Engelen *et al.*, 2016]. Excessive sliding of these components can pose both safety and economic risks during an earthquake. Large sliding displacements can lead to the blocking of exit routes, contents sliding off edges, and can increase the chance of collision with other building contents. Large sliding velocities contributing to large momentum of sliding components at impact can also lead to injury of building occupants or damage to the components themselves. The seismic performance of slender unanchored nonstructural components that are free to rock can also pose significant safety and economic risks during an earthquake. Since rocking components were first studied by Housner [1963], they have gained increased attention in proceeding studies [Yim *et al.*, 1980; Shenton, 1996; Makris and Roussos, 1998 & 2000; Makris and Konstantinidis, 2003]. Overturning of rocking components can have severe consequences, as heavy rocking components such as cabinets, fridges or shelving units, can cause serious injury and large accelerations at overturning impact can lead to damage to the rocking components and the contents they hold [Filiatrault *et al.*, 2004; Konstantinidis and Makris, 2009, 2010; Linde, 2016].

1.3 Objectives

The purpose of this study is to evaluate the performance of nonstructural components in CRSBFs with differing base rocking joint and frame designs, and to compare the overall performance of nonstructural components between buildings using the CRSBF and BRBF systems. Also studied is whether the concerns surrounding nonstructural component performance in CRSBFs, that are discussed earlier, truly have a significant impact on

nonstructural component demands. In Chapter 2, two different CRSBFs were designed for buildings with 3, 6, and 12-storeys, along with a BRBF at each building height. The systems were designed to achieve similar median peak interstorey drift performance, as described in Section 2.4, thus allowing for a fair comparison of demands on acceleration-sensitive nonstructural components. The nonstructural components were analyzed using a cascading analysis approach, as described in Section 6.1, where the absolute floor accelerations obtained from nonlinear time-history analyses of the structures were used as inputs in order to calculate the response of each component. To provide an assessment of a broad range of nonstructural components in each system, three types of nonstructural components were analyzed in this study: 1) anchored components which were assessed by means of elastic floor response spectra; 2) unanchored stocky components which were assessed by sliding displacement and velocity spectra; and 3) unanchored slender components which were assessed by rocking spectra.

Chapter: 2 Design of Seismic Force Resisting Systems

Two CRSBFs and one BRBF structure were designed for building heights of 3, 6, and 12 storeys. The structures were located in the Los Angeles area on site class D soil, as per ASCE 7-16 [2016]. The short-period site coefficient, F_a , and the long-period site coefficient, F_v , were 1.0 and 1.7, respectively. The site had a mapped short-period MCE_R spectral acceleration of $S_S = 1.5$ g and an MCE_R spectral acceleration of $S_1 = 0.6$ g at a period of 1 s. The long-period transition period of the site was $T_L = 8.0$ s. The building was designed for a design basis earthquake (DBE), i.e., 2/3 of the intensity of a 2% in 50 year maximum considered earthquake (MCE), and the resulting 5% damped elastic response spectrum is shown in Figure 2.1 (a). The structural layout of the gravity framing, and brace configurations of the 3-storey CRSBF and BRBF structures are shown in Figure 2.1 (b). The structure had equal storey heights of 4.57 m and equal bay widths of 9.14 m. Each CRSBF consisted of a chevron braced frame that lay inside the columns of the gravity framed bays and was designed to have a width of 80% of the bay width. Each BRBF consisted of two braced bays per frame with braces that extended the full width of each bay and were pinned to gusset plates at the beam-column joints. The number of frames used for each building height and for each lateral force resisting system is shown in Table 2.1 and Table 2.2. The seismic weights of the floor and roof levels were 10,090 kN and 6,440 kN, respectively.

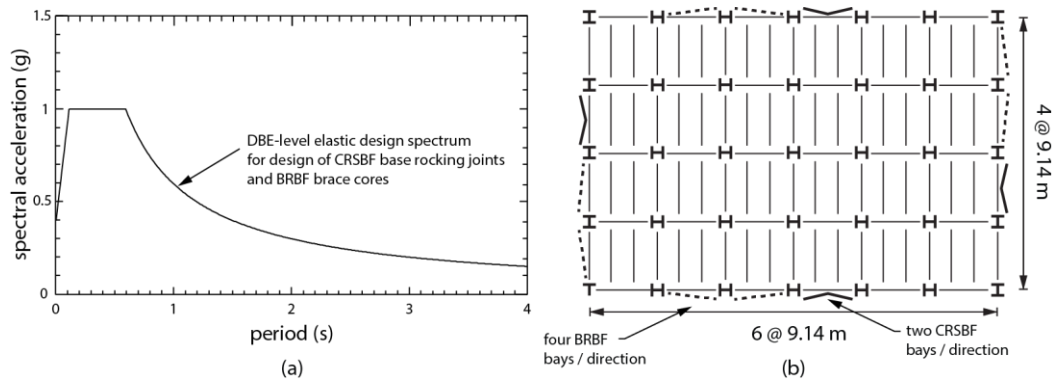


Figure 2.1 (a) DBE elastic response spectrum at 5% damping, and (b) 3-storey structural floor plan

Although the building was assumed to be a Risk Category II structure, a peak allowable seismic interstorey drift of 1.5% was chosen for the designs rather than the 2% allowable drift prescribed in Table 12.12-1 of ASCE 7-16 [2016]. The reason for this design choice was that if CRSBFs are to be used as a high-performance system, it may also be likely that designers would seek a higher level of drift performance.

2.1 Design of CRSBFs Part I: Base Rocking Joint Design

The design of CRSBFs has typically been broken into two distinct steps: design of the base rocking joint, and capacity design of the frame members [Wiebe and Christopoulos, 2015a; 2015b]. The design methodology set out by Wiebe and Christopoulos [2015a] was used in order to design the base rocking joints of the CRSBFs. The first step in the base rocking joint design process was selecting the force reduction factor, R , the energy dissipation ratio, β (equal to two times the ratio of the overturning moment resistance provided by the energy dissipation to the total overturning moment resistance provided by the base rocking joint design), and the fundamental period of the grounded CRSBF. The initial R factor for each design in this study was taken as $R = 8$. This value has been recommended by several researchers [Ma *et al.*, 2010; Roke, 2010; Eatherton *et al.*, 2014] and is also the maximum

force reduction factor provided in ASCE 7-16 [2016] for any seismic force resisting system. However, other researchers have shown that CRSBFs can meet drift and collapse criteria at even larger R factors [Wiebe and Christopoulos, 2015a; Steele and Wiebe, 2017] and therefore design iterations with R values of up to 20 were considered. Two different values of β (25% and 90%) were used for each building height, as listed in Table 2.1, in order to compare demands in two CRSBFs with wide variations in supplemental energy dissipation. An initial prestressing ratio, the ratio of the initial stress of the prestressing to the ultimate stress of the prestressing, of 15% was also targeted for all CRSBF designs, although this design objective needed to be altered for the 12-storey CRSBFs as discussed in Section 2.5. In order to get a first estimate of the CRSBF fundamental period, the equation developed by Kwon and Kim [2010] for concentrically braced frames was used. After an initial estimate, the fundamental period calculated from the OpenSees [PEER, 2015] model described in Chapter 3 was used in the base rocking joint design process.

First, the code reduced lateral forces acting on the structure were determined using the equivalent lateral force procedure in ASCE 7-16 [2016]. The base rocking joint must be designed to resist the overturning moment caused by the code reduced lateral forces. Since the CRSBFs analyzed in this study were assumed to be decoupled from the gravity loads of the floor diaphragms, the base rocking moment $M_{b,rock}$ is equal to the sum of the moment resistance provided by the self-weight of the rocking frame members (M_W), a friction interface energy dissipation device (M_{ED}), and the prestressing anchoring the frame to the foundation (M_{PT}), as shown in Equation (1):

$$M_{b,rock} = M_W + M_{ED} + M_{PT} \quad (1)$$

For the initial design, M_W was assumed to be 5% of $M_{b,rock}$ [Wiebe and Christopoulos, 2015a], while M_{ED} was calculated using Equation (2):

$$M_{ED} = \frac{M_{b,rock}\beta}{2} \quad (2)$$

Since the moment arm of the friction interface energy dissipation device to the rocking toe was known, the necessary activation force of the friction interface device was calculated as the force needed to achieve an overturning moment resistance of M_{ED} provided by the energy dissipation. A friction interface was chosen as it was representative of an energy dissipation device with a full hysteretic response, such as friction or yielding elements. The remaining overturning moment resistance was provided by M_{PT} . Again, the moment arm from the prestressing cable to the rocking toe was known based on whether the prestressing was provided at both columns or at the centre of the frame and was used to calculate the initial prestressing force needed to provide uplift resistance. The number of prestressing tendons was then chosen based on the desired prestressing ratio and/or base rocking joint rotation desired before the prestressing would yield.

A few checks were made to ensure adequate performance of the base rocking joint design. Zhang *et al.* [2018] found that a small secondary stiffness of a SDOF flag-shaped hysteretic system does not have a detrimental impact on peak displacements as long as the secondary stiffness is not negative. Therefore, to estimate the secondary stiffness of the base rocking joint design, the normalized secondary stiffness of the base rocking joint, $\bar{\alpha k}$, was checked using Equation (3) [Wiebe and Christopoulos, 2015a]:

$$\bar{\alpha k} = [(E_{PT}A_{PT}/L_{PT})d_{PT}^2 - W_{trib}H_w]/(M_eH_e^2) \geq 0 \quad (3)$$

where E_{PT} is the Young's modulus of the prestressing tendons, A_{PT} is the total cross-sectional area of the prestressing, L_{PT} is the length of the prestressing, d_{PT} is the moment arm of the prestressing to the rocking toe, W_{trib} is the seismic weight tributary to the CRSBF, H_W is the vertical centre of mass of the floor diaphragms, and M_e and H_e are the effective mass and height, respectively, of the CRSBF idealized as an SDOF [Priestley *et al.*, 2007]. Ratcheting of the system can also occur when the self-centring provided by the self-weight of the frame and prestressing is not large enough to overcome the slip load of the energy dissipation device [Eatherton *et al.*, 2014] and therefore the maximum amount of energy dissipation provided must be checked against Equation (4):

$$W_{self} + \sum PT_{initial} \geq \sum ED_{max} \quad (4)$$

where W_{self} is the combined self-weight of the frame members, $PT_{initial}$ is the initial prestressing force, and ED_{max} is the maximum expected force in the friction interface energy dissipation device. Finally, the resistance of the CRSBF to overturning at the maximum allowable base rocking joint rotation in order to prevent collapse, θ_{max} , was also checked using Equation (5):

$$W_{self}d_W + \sum (ED d_{ED}) + \sum (PT_{\theta_{max}}d_{PT}) > W_{trib}H_W\theta_{max} \quad (5)$$

where d_W is the moment arm of the self-weight of the frame to the rocking toe, ED is the activation force of the friction energy dissipation device, d_{ED} is the moment arm of the energy dissipation device to the rocking toe, and $PT_{\theta_{max}}$ is the force in the prestressing at the maximum allowable base rocking joint rotation in order to prevent collapse. Upon completion of the preliminary base rocking joint design, the frame members of the CRSBF were designed based on the method described in Section 2.2, and the actual self-weight and

fundamental period of the CRSBF were calculated using the OpenSees [PEER, 2015] CRSBF model. The base rocking joint design was then iterated based on the new self-weight and period until the capacity design procedure converged on an identical frame design. Section 2.4 discusses further iteration of the designs based on the interstorey drift results of the nonlinear time-history analysis.

2.2 Design of CRSBFs Part II: Capacity Design of Frame Members

The dynamic capacity design procedure developed by Steele and Wiebe [2016] was used to design the CRSBF frame members. The dynamic procedure combines the force effects from the frame rocking to its ultimate base rotation in its fundamental mode with the force effects acting on the frame members due to higher-mode vibrations as the CRSBF rocks. This procedure requires an elastic model of the CRSBF that is only pinned about one of its toes, to simulate the boundary conditions of the frame during rocking rather than the grounded phase. The force effect of the prestressing is captured by attaching a spring element at the top of the frame that has an equivalent axial stiffness to the prestressing cable and by applying the corresponding prestressing force acting on the frame. The friction interface energy dissipation device is captured by adding a point load to the base of the column where the device is attached to the foundation. The schematic of the elastic model during rocking is shown in Figure 2.2 (a).

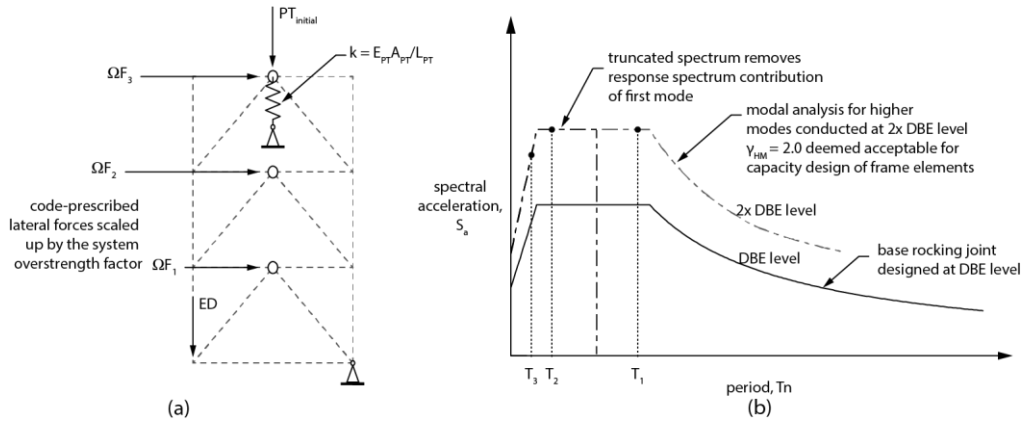


Figure 2.2 Capacity design: a) elastic model of CRSBF rocking about its toe for modal analysis, b) DBE response spectrum and truncated spectrum amplified for higher modes [after Steele and Wiebe, 2016]

The capacity forces for the frame members are then determined through a two-step process. The forces experienced by the frame members as the frame rotates to its ultimate rotation in its fundamental rocking mode are captured by applying the code reduced lateral forces amplified by the overstrength factor of the CRSBF, Ω , shown in Equation (6):

$$\Omega = \frac{M_{b,max}}{M_{b,min}} \quad (6)$$

where $M_{b,max}$ is the maximum base overturning moment resistance provided by the base rocking joint as the CRSBF rocks to its ultimate base rotation before experiencing fracture of the prestressing. $M_{b,min}$ represents the base overturning moment experienced by the CRSBF due to the code reduced lateral forces, which is the moment that the base rocking joint was designed to resist. The amplified lateral forces are then applied to the elastic model of the frame during rocking and member forces are calculated.

The next step in the capacity design procedure is capturing the forces due to vibration of the frame at higher modes which is performed through a truncated modal analysis procedure. Using the natural periods of the model described above, the response spectrum

is truncated to only consider the higher modes, as shown in Figure 2.2 (b). Because the higher-mode effects have been shown to have a significant impact on the frame member forces, the DBE response spectrum is amplified by a higher-mode factor, γ_{HM} , to ensure adequate elastic performance of the frame. Some studies have shown that considering the response spectrum at the maximum considered earthquake (MCE) level is adequate for preventing collapse of the CRSBF [Steele, 2019], thus resulting in $\gamma_{HM} = 1.5$. However, in this study the DBE response spectrum was amplified by $\gamma_{HM} = 2.0$ for the truncated modal analysis. This factor was chosen manually, and was generally successful in ensuring that during the nonlinear time-history analyses at least 84% of records did not experience yielding or buckling of the frame members, while also avoiding substantial overdesign of the members, as shown in Chapter 5.

2.3 Design of BRBFs

The design of the BRBF structures was also broken into a two-step process, where the BRB cores were first designed to resist the code reduced lateral forces based on the equivalent lateral force procedure in ASCE 7-16 [2016], followed by a capacity design of the columns in the BRBF to remain elastic. In the initial design, $R = 8$, and the fundamental period was estimated based on the approximate fundamental period equation provided for BRBFs in ASCE 7-16 [2016]. After the initial design, if the target design drift criterion was not met, the R factor was reduced proportionately to the overdesign factor of the BRB cores compared to the original factor of $R = 8$, and the new fundamental period was determined from the BRBF OpenSees model. The BRBs were assumed to be pin connected to gusset plates at the beam-column connection of each braced bay. The 3, 6, and 12-storey BRBFs

consisted of two frames with two braced bays in each frame. The BRB core areas were designed to resist the axial forces caused by the code reduced lateral forces based on the assumed yield strength of 287 MPa. Although the gusset plate connections were not explicitly designed in this study, they were considered in the overall stiffness of the BRBs during design and modeling. It was assumed that both gusset plates on either end of the BRBs took up a combined 15% of the work point to work point distance between the beam-column-brace joints of each bay. The gusset plates were assumed to act as axially rigid. Also not explicitly designed or modeled, but considered in the overall stiffness of the BRBs, were the BRB fins that connect the BRB cores to the pin connection at the gusset plates. It was assumed that the fin connections took up a combined 20% of the distance between the pin connections, and the area of the fins was assumed to be four times as large as that of the BRB cores. This resulted in BRB core yield length ratios (the ratio of the actual length of the BRB core to the work point to work point distance of the hypotenuse of the braced bay) of 0.68.

In practice, BRBs are typically proprietary elements that are designed and tested for qualification by the manufacturer. This forces researchers to make assumptions on the yield strength, secondary stiffness and overstrength of the BRB cores in tension and compression. Therefore, to estimate the probable yield stress and tensile and compressive overstrength of the BRBs designed and modeled in this study, a study by Saxey and Daniels [2014] that characterized the overstrength factors for BRBs into regression equations based on the results of laboratory tests on 39 full scale specimens was followed. A yield strength of 287 MPa was chosen for the BRBs, as it was the midpoint of the range of yield strengths

tested in the Saxey and Daniels study. Determining the probable forces in tension and compression that the BRBs will apply to the frame at the maximum expected displacement is necessary in designing the capacity protected elements of the BRBF, such as the brace connections and columns. The probable tensile and compressive forces of the BRB cores can then be expressed in terms of yield stress, area and the determined overstrength factors, as shown in Equations (7) and (8):

$$T_{probable} = \omega R_y \sigma_{ysc} A_{core} \quad (7)$$

$$C_{probable} = \omega \beta_{comp} R_y \sigma_{ysc} A_{core} \quad (8)$$

where σ_{ysc} is the yield stress of the BRB core, A_{core} is the cross-sectional area of the BRB core, and $R_y = 1.0$ as it is assumed in this study that the yield strength of the BRB cores is known through coupon testing. Saxey and Daniels [2014] provided regression equations for determining the strain hardening adjustment factor, ω , and the compressive strength adjustment factor, β_{comp} , based on the expected axial strain of the BRB core. The resulting regression equations based on the average of the laboratory tests of only the pinned BRBs are shown in Equations (9) and (10):

$$\omega = 20.625\varepsilon + 1.0413 \quad (9)$$

$$\beta_{comp} = 10.366\varepsilon + 0.9981 \quad (10)$$

In the capacity design of the columns, it was assumed that each BRB reached its probable tensile or compressive force at a strain that was twice the strain experienced by the BRB cores at the target design drift of 1.5%. These forces were then applied to the columns in the two-bay braced frame and the probable loads were combined with the gravity forces acting on each column. Each column was designed according to the standards of AISC 360-16 [2016].

2.4 Design Iteration Based on Nonlinear Time-History Analysis

The designs of the seismic force resisting systems were iterated in order to reach similar median peak interstorey drifts based on the nonlinear time-history analyses, so that a fair comparison of acceleration-sensitive components could be made from the perspective of similar displacement-sensitive component performance between the two systems. Therefore, following the design of each CRSBF and BRBF, nonlinear time-history analyses were conducted, and the median peak interstorey drift from the suite of ground motions was calculated at each storey level. If the median peak interstorey drift at the critical storey was calculated to be higher than the target design drift, or lower than the target design drift by more than 5%, the design was iterated. For the CRSBF, drifts can be controlled by altering the base overturning moment that causes uplift of the frame, the amount of energy dissipation provided in the base rocking joint design, or the fundamental period of the frame. Since the designs considered in this study were to be compared by controlling different amounts of energy dissipation, and increasing frame member stiffness would be considered to be a more costly design iteration, the CRSBF designs were iterated by altering the rocking moment of the base rocking joint design (i.e. increasing or decreasing R). The BRBF designs were iterated by increasing the area of the brace cores in order to control drifts, which reduced the effective R value of the system. Once the CRSBF base rocking joints and BRB cores were redesigned, and a new design of the capacity protected elements was completed, the ground motions were rescaled, and time-history analyses were reconducted until the desired median peak interstorey drift was satisfied.

2.5 Final Design Parameters

The final design parameters for the CRSBFs and the BRBFs are shown in Table 2.1 and Table 2.2, respectively. 3S- β 25 represents the 3-storey CRSBF designed with $\beta = 25\%$. Also shown in Appendix A are the final designed frame members of the CRSBFs and BRBFs.

Table 2.1 Final CRSBF structural design parameters

Design	# Frames	R	β	η	# Strands	PT Location	T_1 (s)	T_2 (s)	T_3 (s)
3S- β 25	2	10.32	0.25	0.15	72	Middle	0.39	0.13	0.09
3S- β 90	2	13.91	0.90	0.15	33	Middle	0.48	0.16	0.12
6S- β 25	4	17.78	0.25	0.15	67	Middle	0.82	0.25	0.15
6S- β 90	4	18.82	0.90	0.15	33	Middle	0.94	0.29	0.16
12S- β 25	4	5.25	0.25	0.40	81	Columns	1.89	0.50	0.27
12S- β 90	4	16.84	0.90	0.09	46	Columns	2.26	0.55	0.29

Table 2.2 Final BRBF design parameters

Design	# Frames	Braced Bays Per Frame	R	T_1 (s)	T_2 (s)	T_3 (s)
3S	2	2	5.41	0.72	0.32	0.20
6S	2	2	5.18	1.25	0.50	0.32
12S	2	2	4.30	2.27	0.84	0.49

For the 3-storey CRSBFs, $M_{b,rock}$ was reduced in order to bring the peak median drift up to 1.5%, resulting in $R = 10.32$ and $R = 13.91$ for the two designs with $\beta = 25\%$ and $\beta = 90\%$, respectively. In order to successfully satisfy the design requirement of maintaining median peak interstorey drifts within 5% of the target 1.5% interstorey drift, the result of using much less supplemental energy dissipation in the 3S- β 25 design was a higher designed $M_{b,rock}$, and also a stiffer capacity designed frame than the 3S- β 90 design. This suggests that the most economical way to control the drifts of CRSBFs may be to provide as much supplemental energy dissipation as possible, thus reducing frame section sizes and

prestressing strands and detailing. Placing the prestressing at the middle of the frame was necessary in order to avoid the large strains that the tendons would have experienced by placing the prestressing at the columns, which uplift twice as much as the centre of the frame. This becomes even more important for the 3-storey structure which has a shorter prestressing cable relative to the other height CRSBFs. In order to resist the initial compression imparted in the braces from the prestressing at the top of the CRSBF, the third storey braces were designed to be much stiffer than the braces in the storeys below.

The final 3-storey BRBF design had a force reduction factor of $R = 5.41$. Although the R factor was much smaller in the 3-storey BRBF than the CRSBFs, the fundamental period of the BRBF was markedly longer than the fundamental periods of the two CRSBFs.

The R factors of the two 6-storey CRSBF designs (6S- β 25 and 6S- β 90) ended up being much closer to each other ($R = 17.78$ and $R = 18.82$, respectively) compared to the 3-storey CRSBFs. Similar to the 3-storey CRSBFs, the 6-storey design with the larger $M_{b,rock}$ and less energy dissipation had a stiffer capacity designed frame and placing the prestressing at the middle of the frame resulted in the sixth storey having the stiffest braces.

The 6-storey BRBF design had a final force reduction factor of $R = 5.18$. As previously mentioned, in order to control interstorey drifts, the cross-sectional area of the BRB cores were increased until the median peak interstorey drifts in the critical storey were within 5% (and also below) of the target design interstorey drift of 1.5%, with one caveat. The BRBFs taller than 3 storeys experienced significant interstorey drifts at the top storeys, which meant that the effective R factor of the system needed to be significantly reduced in order

to reduce the median peak interstorey drift below 1.5% at the top storey. This resulted in drastic overdesign of the BRB cores in the remaining storeys. For this reason, the BRB cores were overdesigned by the same factor until the median peak interstorey drifts at the 1st storey fell below the target design drift of 1.5% (which resulted in a 6th storey drift that was still greater than 1.5%). Once this drift performance was achieved at the first storey level, the sixth storey BRB core was manually overdesigned until the median peak interstorey drift at that level was also below 1.5%. This resulted in sixth storey BRBs that were 16% overdesigned based on the core area that would be deemed necessary based on the code reduced lateral force distribution of an $R = 5.18$ design.

The prestressing for the 12-storey CRSBFs was placed at the columns of the frame and ran the full height of the CRSBF. The column location allowed for a lower prestressing force than if placed at the middle of the frame since the moment arm to the rocking toe was larger, but choosing the column location was also made possible by the fact that a longer prestressing cable (due to the taller structure) was not subject to the high strain demands that would be seen for shorter cables (as in the 3- and 6- storey CRSBFs). The design of the 12-storey CRSBFs also required a deviation from the original design objective of maintaining a prestressing ratio of $\eta = 15\%$ for all CRSBF designs. For the 12S- β 25 design, in order to control peak median drifts an $R = 5.25$ was necessary. With a small β and relatively low R factor, the resulting prestressing force for this design was quite high and would have called for an excessively large number of prestressing tendons in order to keep $\eta = 15\%$. For this reason, exceeding a number of prestressing tendons larger than 81 was deemed excessive, and the lowest possible η for the design was $\eta = 40\%$, with 81

prestressing tendons. On the other hand, the 12S- β 90 design had its own challenges in designing the prestressing. Maintaining the same location and length of the prestressing as the 12S- β 25 design, the number of prestressing tendons could not be reduced enough to increase η to the target of 15%. This is because the conservative estimate of the post-uplift stiffness of the CRSBF in Equation (3) would become negative if fewer than 44 tendons were used for the 12S- β 90 design. Therefore, 46 prestressing tendons were chosen and the resulting prestressing ratio was $\eta = 9\%$. Although the 12-storey CRSBFs were not able to be designed with the consistent prestressing ratio of $\eta = 15\%$, overall the prestressing ratio was not expected to have a major impact on altering nonstructural component performance.

The 12-storey BRBF design was iterated until reaching a final force reduction factor of $R = 4.30$. Similar to the 6-storey BRBF design explained above, the cross-sectional areas of the BRB cores were increased until the first storey drifts were below the target interstorey drift of 1.5%. At that point, the 11th and 12th storeys experienced drifts exceeding 1.5%, but reducing the R factor further was not successful in controlling these drifts. Therefore, the 11th and 12th storey BRB cores were manually oversized by 12% and 38% based on the code reduced lateral forces at $R = 4.30$, respectively. Although the design iteration of the top storey braces in the 6- and 12-storey BRBFs was unconventional, the concentration of interstorey drifts at the top storeys of the BRBFs, as shown in Chapter 5, necessitated overdesign in order to ensure that no storey experienced an interstorey drift larger than the allowable design drift. Furthermore, the overdesign of the top storey braces was a conservative design choice, and was not expected deviate the design significantly from an expected median BRBF designed using the equivalent lateral force procedure in ASCE 7-

16 [2016], as the increase in top storey brace stiffness had a minimal impact on increasing the interstorey drifts in the storeys below.

Chapter: 3 Modeling of Seismic Force Resisting Systems

3.1 CRSBF Model

An OpenSees [PEER, 2015] model was used for the nonlinear time-history analyses of the CRSBF system. An example schematic of the CRSBF model for the 3-storey structure is shown in Figure 3.1 (a). The beam, column and brace members were modeled using elastic beam-column elements. An elastic model of the frame members was deemed acceptable since the capacity design procedure ensured that for the majority of ground motions, the frame members remained elastic during the nonlinear time-history analyses (See Chapter 5). The stiffness provided by the gusset plate connections at the beam-column-brace joints was modeled using rigid elements. Although the brace members were assumed to be pin ended to the rigid links of the gusset plates in the calculation of out-of-plane buckling loads, in the 2D model this connection was modeled as fixed in plane. A leaning column was modeled to capture the P-Delta effects acting on the system. The lateral inertial loads were assumed to be transferred from the floor diaphragm (assumed to be rigid) to the CRSBF at the centre nodes of the frame where the chevron braces meet. Therefore, the floor masses were lumped at the nodes of the leaning columns at each storey and the centre joints of the rocking frame were constrained in the horizontal direction to the leaning column nodes. The prestressing was modeled using a corotational truss element, combined with an initial stress material in parallel with a multi-linear material with a yield strain of 0.0083 and yield stress of 1670 MPa. The ultimate strain and stress of the prestressing were 0.013 and 1860 MPa, respectively. Depending on the location of the prestressing, the prestressing

element was attached to either the centre node of the chevron braces or the beam-column-brace joint at the designed storey. The prestressing was anchored to the foundation using a tension-only gap element which worked as a hook connection that allowed the prestressing to develop tensile stresses but did not provide a reaction force when the prestressing truss element attempted to develop compression stresses. The friction interface energy dissipation devices were located at the bases of each column and were modeled using an elastic perfectly plastic element with an essentially infinite first stiffness which allowed the friction device to activate once the slip load had been surpassed, and a constant friction force was applied in the secondary stiffness range. The friction interface energy dissipation elements at the column bases were modeled using elastic-no tension horizontal and vertical gap elements that were essentially rigid in compression. These elements provided the foundation supports to the rocking frame while also allowing the frame to freely uplift during rocking. A Rayleigh damping model with damping factors proportional to the tangent stiffness and mass of the system was used by applying an inherent damping ratio of 2% to the first two modes of the CRSBF. Full details of the OpenSees model can be found in Steele and Wiebe [2016].

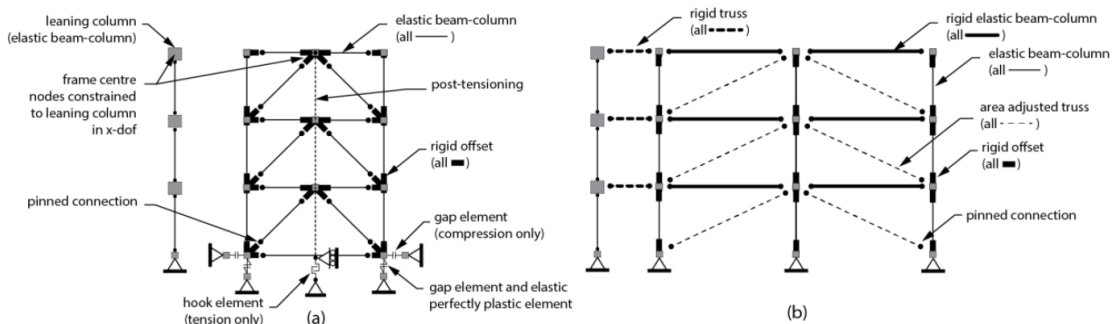


Figure 3.1 OpenSees model schematics: (a) CRSBF [after Steele and Wiebe, 2016], (b) BRBF

3.2 BRBF Model

The BRBFs were also modeled in OpenSees [PEER, 2015], and a schematic of the model is shown in Figure 3.1 (b). Similar to the CRSBF, the columns were modeled as continuous, with elastic beam-column elements and rigid offsets mimicking the gusset plate beam-column-brace connections. The beams were modeled as axially rigid in order to represent the assumed rigid floor diaphragm. A leaning column was also provided and was connected to the frame through axially rigid truss elements.

The BRBs were modeled to match the equivalent lateral stiffness and probable forces discussed in the assumptions of the BRBF design in Section 2.3. The BRBs were modeled using truss elements that were pinned to the beam-column-brace joints of the frame. In order to represent the true axial stiffness of the BRBs, the area of the truss elements was increased based on the equation for equivalent stiffness of springs in series. Based on the assumed gusset plate length, and BRB fin connection length and area, the area of the BRB truss elements were increased by a factor of 1.3841 times the designed BRB core area. In order to provide further validation to the equivalent stiffness method used, a separate BRB brace model was developed. In this model the gusset plates and their lengths were explicitly modeled with rigid elements and the BRB fins were modeled with their exact lengths and the assumed area of 4 times the BRB cores, and were pinned to the gusset plate elements. The BRB core itself was modeled with two elements in parallel that were fixed to the fin connections. The first element was modeled with a force-based beam-column element where the cross-sectional area was built out of fibre sections. This element represented the true axial stiffness and strength of the BRB core. The second element in parallel was an

elastic beam-column element that was modeled with essentially zero cross-sectional area but was essentially rigid in flexure. The purpose of this element was to take any flexure that the force-based beam-column element might take while not contributing at all to the axial stiffness or strength of the core. This was done to ensure that the BRB core could act as a truss element while still having the fixed end conditions of the core to the fin connectors. The hysteretic response of this model was compared to that of the equivalent truss element model as shown in Figure 3.2. The cyclic pushover of the BRBs based on the protocol for qualification of BRBs described in AISC 341-16 [2016] showed nearly identical agreement between the hysteresis loops, with the exception being that the parallelized beam-column BRB model experienced slightly larger yield strains at each post yield cycle due to the fact that the full length of the truss element experiences the strain of each interstorey drift cycle. Nevertheless, both models experienced nearly identical yield strains and stress at any given strain in the hysteresis loop. Therefore, the equivalent truss element model was used in the nonlinear time-history analyses due to its simplicity and economic run time, while not being expected to hinder to accuracy of the results.

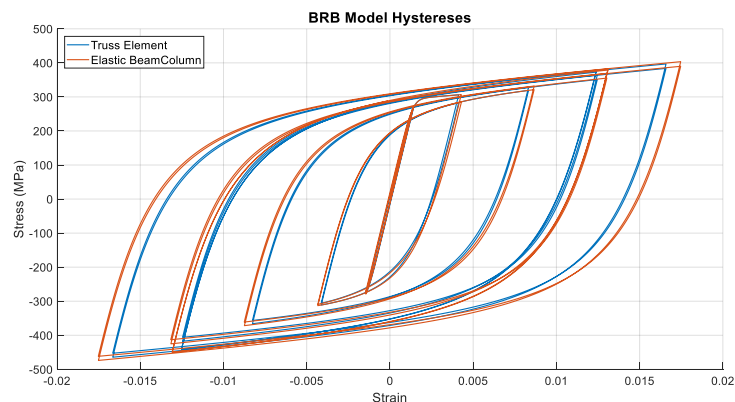


Figure 3.2 Calibration of BRB Brace Hysteresis in OpenSees comparing the equivalent truss element to parallelized beam-column elements

The hysteretic response of the BRBs was calibrated based on the results of the regression equations characterizing BRB overstrength factors developed by Saxey and Daniels [2014]. The truss elements were modeled using the Steel02 Giuffré-Menegotto-Pinto material in OpenSees. The elastic modulus of the material was assumed to be 200 GPa and the secondary stiffness of the steel was assumed to be 2% of the elastic stiffness. The Steel02 material provides separate isotropic hardening parameters in tension and compression that increase the yield envelope of the hysteresis based on the specified portion of the yield strength. Because the overstrength regression equations calculated by Saxey and Daniels were based on the peak brace stresses experienced during experimental testing of BRBs that typically go through the loading protocol for qualification of BRBs described in AISC 341-16 [2016], the isotropic hardening parameters in tension and compression were chosen based on a trial and error method whereby the modeled BRB was put through the loading protocol for BRB qualification. The hardening parameters, which represent the increase in the tension or compression envelope in proportion to the yield stress in cycles post yielding, were adjusted until the modeled BRB strengths in tension and compression at the furthest loading cycle, matched tensile and compressive overstrength estimated by the regression equations in Saxey and Daniels. The final isotropic hardening parameters in tension and compression were about 0.032 and 0.066, respectively. Because the target drift of the design was 1.5%, the BRB core strain at twice the design drift was calculated and this strain was used in the regression equations to calculate BRB overstrength stresses of 396.5 MPa and 464.1 MPa.

Chapter: 4 Ground Motion Selection and Scaling

The FEMA P695 Far-Field record suite of 44 ground motions (two horizontal directions from 22 earthquake motions) [ATC, 2009] was used in the nonlinear time-history analysis. Prior to any scaling, normalization factors for each ground motion are provided in FEMA P695 that normalize the records to their peak ground velocities in order to remove unwanted variability between records due to differences in magnitude, site conditions, location and type of earthquake, while still maintaining the record-to-record variability needed to capture a wide range of response amplitudes and frequencies. Although FEMA P695 calls for the ground motion suite to be scaled to the fundamental period of the structure, this method would result in different scale factors for each design, making it difficult to draw comparisons between nonstructural component demands. Therefore, once the ground motions were normalized, for each separate building height the entire record suite was scaled by one scale factor for each set of 3, 6 and 12-storey designs, such that the mean squared error of the median spectral acceleration of the suite compared to the DBE spectral acceleration spectrum was minimized within a period range of 0.2 times the smallest of the fundamental periods of the three designs to two times the largest of the fundamental periods of the three designs. This was a modification of the scaling method suggested in ASCE 7-16 [2016] which scales within the aforementioned range of periods for a single design. Scaling within this range of periods not only provided a ground motion suite representative of all three designs at a given storey height, but also ensured that each design at a given structure height experienced identical intensities for the purpose of comparing

nonstructural component demands. The scale factors for the 3, 6, and 12-storey structures were 1.43, 1.49 and 1.68, respectively, and an example of the scaled response spectrum is shown in Figure 4.1.

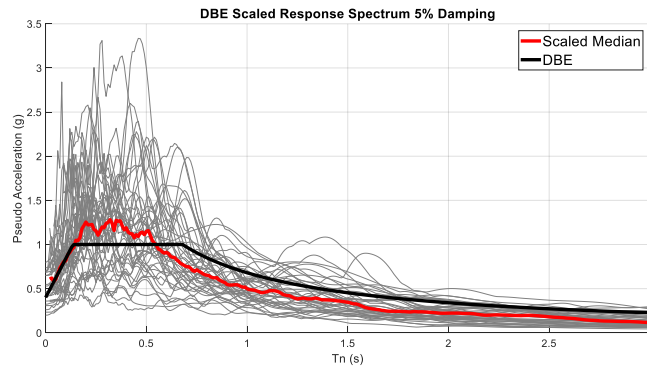


Figure 4.1 3-Storey DBE response spectrum and scaled ground motions

Chapter: 5 Nonlinear Time-History Analysis Structural Results

The interstorey drift profiles, residual interstorey drifts and brace forces for the 3, 6 and 12-storey structures are shown in Figure 5.1, Figure 5.2, and Figure 5.3, respectively.

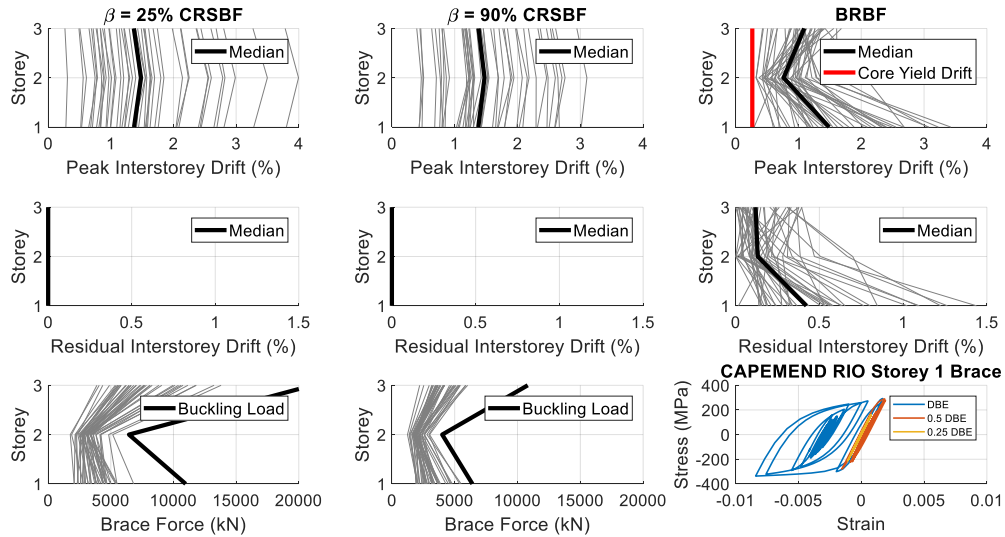


Figure 5.1 3-storey CRSBF and BRBF nonlinear time-history analysis structural results

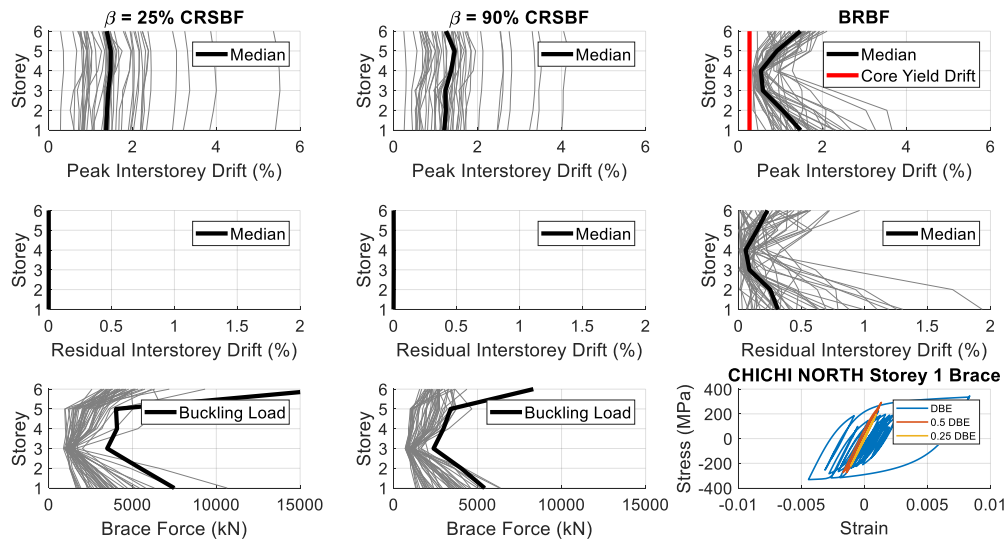


Figure 5.2 6-storey CRSBF and BRBF nonlinear time-history analysis structural results

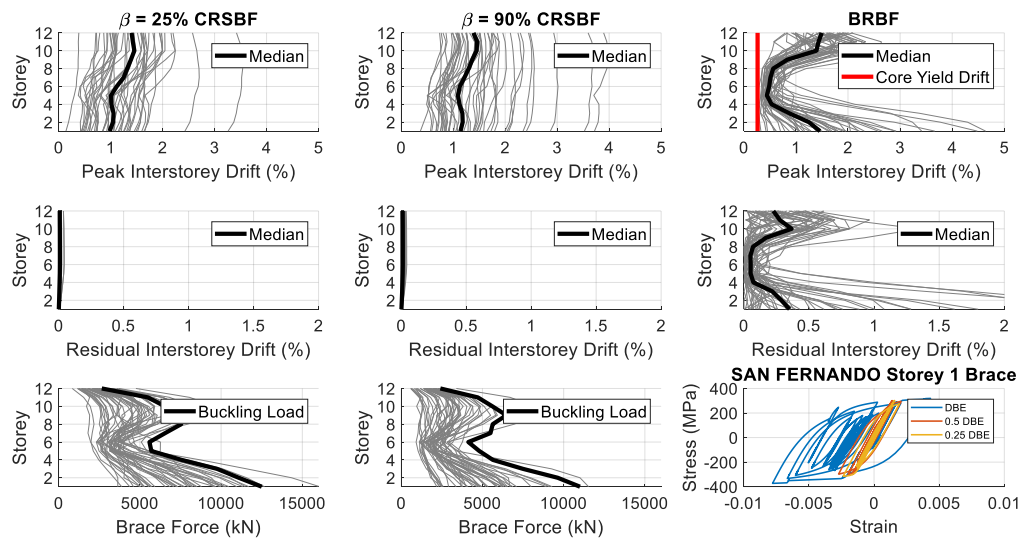


Figure 5.3 12-storey CRSBF and BRBF nonlinear time-history analysis structural results

The fundamental rocking mode dominates the displacement response of the CRSBFs. This is evident especially in the 3- and 6-storey CRSBFs which have nearly uniform drift profiles. In the 12-storey CRSBFs, although the interstorey drifts are still more uniform than in the BRBF throughout the height of the structures, the median interstorey drifts tend to increase from the lower to higher storeys of the CRSBFs. As the height of the CRSBF increases, the rocking frame becomes more flexible and although the rocking mode still dominates the displacement response, the deformations of the frame members contribute more to the interstorey drifts for the taller, more flexible frame. On the other hand, the BRBFs experience a much less uniform drift profile, where interstorey drifts seem to concentrate at the lower and upper storeys rather than the middle storeys. The BRB cores are designed with identical overstrength factors (with some exceptions, see Section 2.5) based on the code reduced lateral forces. This results in significant overstrength and markedly lower interstorey drifts in some of the middle storeys of the BRBFs. Nevertheless,

the results showed that yielding still occurred at all storeys, for all BRBF designs, at DBE intensity. Therefore, in terms of drift profile, there are both advantages and disadvantages that can be argued for both systems. The uniform drift profile of the CRSBF can be seen as an advantage to designers who do not need to worry about drifts concentrating at any one storey. The designer also has much more control over reducing the drift response of the CRSBF as increasing the rocking moment of the system may result in marginal changes in system cost (as long as the capacity design of the frame members is not significantly changed), whereas greatly increasing the stiffness of the BRB cores may be unfeasible. However, as long as the redundancy of the BRBF is not so great as to significantly drive up the cost of the system, the non-uniform drift profile of the BRBF can be seen as an advantage, as only a few of the storeys would experience demands on displacement-sensitive nonstructural components that reach the design limit.

The residual drift performance between the two systems shows one of the main structural advantages of using a CRSBF. As shown at all structure heights, the self-centring capabilities of the CRSBF brought the residual displacement of the system to essentially zero at the DBE level. Conversely, for the BRBF structures the largest median residual interstorey drifts experienced at any storey were 0.38%, 0.34% and 0.39% for the 3, 6, and 12-storey structures, respectively. Furthermore, the percentage of ground motions that caused at least one storey to experience a residual drift of greater than 0.5% (a value that can suggest it is more feasible economically to completely demolish and reconstruct the structure [McCormick *et al.*; 2008]) was about 45%, 50%, and 66% in the 3, 6, and 12-storey BRBFs, respectively. The large percentage of ground motions with excessive

residual drifts in the BRBF could play an important role in the comparison of nonstructural component performance between CRSBFs and conventional seismic force resisting systems as nonstructural component performance may not have a significant impact on the expected losses of the building if significant reconstruction or demolition is necessary.

Figure 5.1, Figure 5.2, and Figure 5.3 also show the peak compressive brace force experienced in the CRSBFs at each storey, and the corresponding buckling loads of the braces. The results show that the capacity design procedure was successful in maintaining an 84th percentile of braces remaining elastic during the nonlinear time-history analyses, with the exception of the 12S- β 25 design. For the 3-storey CRSBFs, no ground motion produced brace forces large enough to exceed the buckling load of any member for either design. For the 6-storey CRSBF designs, no more than two out of 44 ground motions caused brace buckling at any storey in the 6S- β 25 design and no more than six ground motions caused brace buckling at any storey in the 6S- β 90 design. For the S12- β 90 CRSBF, no more than three ground motions caused a brace to buckle at any one storey. However, for the 12S- β 25 design, the 10th storey had eight ground motions that caused brace buckling, and the 12th storey had 13 ground motions that caused braces buckling. Nevertheless, brace buckling still did not occur in a majority of the ground motions and in terms of collapse capacity, Steele [2019] has shown that CRSBFs can achieve adequate collapse performance even with an average number of braces buckling. Therefore, as the purpose of this study is to analyze the performance of nonstructural components, the use of a model with elastic beam-column brace elements is not expected to have a significant impact on the drift or

acceleration performance of nonstructural components even in the S12- β 25 design, especially when analyzing these components at an average level.

Finally, the hysteretic responses of the first storey BRBs are also shown in Figure 5.1, Figure 5.2, and Figure 5.3, for ground motions that experienced near median interstorey drift demands at the DBE level. The results show that at DBE level the BRB cores experienced significant yielding, whereas at $\frac{1}{4}$ DBE intensity the 3- and 6-storey BRBFs experienced no yielding at the first storey and the first-storey BRBs in the 12-storey BRBF just barely reached their yield stress for a few cycles. The impact of the amount of BRB yielding on nonstructural component performance is discussed further in Chapter 6.

Chapter: 6 Performance of Nonstructural Components

6.1 Overview of Nonstructural Component Analysis Procedure

As similar median peak interstorey drifts were achieved for each of the designs, displacement-sensitive nonstructural component performance was chosen as a controlling variable in the comparison of the nonstructural component performance between the various structures, and comparisons of the demands on anchored and unanchored components that were susceptible to the acceleration of each floor were used to assess the overall nonstructural component performance. The three types of components studied were acceleration-sensitive anchored components, unanchored sliding components and unanchored rocking components. A cascading analysis approach was used to obtain the response of each component, which involved applying the absolute floor accelerations, obtained from the nonlinear time-history analyses at each storey level, to each of the components. Because the CRSBFs analyzed in this study were designed as decoupled from the gravity system, vertical accelerations caused by the CRSBF uplifting and rocking are not expected to be transferred to the floor diaphragms [e.g. Wiebe *et al.*, 2013], and therefore only lateral floor accelerations were considered in this study. In addition, no vertical components of excitation were applied to the structure at the ground level during the nonlinear time-history analyses. The idealized version of each component type is shown in Figure 6.1.

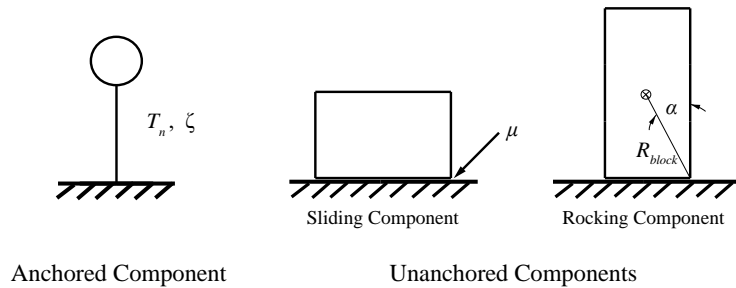


Figure 6.1 Idealized anchored and unanchored nonstructural components

The performance of acceleration-sensitive anchored components was assessed by means of elastic floor spectra of peak pseudo-acceleration, with an assumed viscous damping of $\zeta = 2\%$. Although a viscous damping of $\zeta = 5\%$ has been commonly used for nonstructural components, Kazantzi *et al.* [2018] mentioned that the limited research on this parameter suggests that viscous damping in nonstructural components can lie closer to the $\zeta = 1\text{-}3\%$ range for many components. Therefore, in order to obtain a conservative estimate of the damping experienced by a wide range of anchored components, a viscous damping of $\zeta = 2\%$ was chosen. Furthermore, while absolute acceleration floor spectra may be appropriate for assessing the functional vulnerability of acceleration-sensitive components, e.g. anchored components housing electrical, circuit, or chemical components that are acceleration-sensitive, the focus of this study is on demands imposed on the base anchorage of the anchored nonstructural components, for which pseudo-acceleration is the appropriate demand parameter. Nevertheless, because a viscous damping of $\zeta = 2\%$ was used, the differences between the pseudo-acceleration floor spectra generated in this study, and the absolute acceleration floor spectra were expected to be minimal.

A rigid block that was free, and stocky enough, to slide without rocking was used to determine the demands on sliding components. The block was subjected to the absolute

accelerations of each floor. Coulomb friction was assumed to represent the applied friction force to the block from the interface with the floor. The static and kinetic Coulomb friction coefficients, μ , were assumed to be identical for simplicity, as previous studies have shown that considering the difference between the static and kinetic coefficients of friction in the Coulomb friction model does not have a major impact on peak sliding displacements [Chaudhuri and Hutchinson, 2006; Konstantinidis and Makris, 2009]. The equation of motion governing the response of the rigid sliding block, during sliding, is shown in Equation (11):

$$\ddot{u} + (\mu g)\text{sgn}(\dot{u}) = -\ddot{u}_{floor,x} \quad (11)$$

where u is the relative displacement of the rigid block to the floor, g is the acceleration due to gravity, and $\ddot{u}_{floor,x}$ is the absolute horizontal acceleration of the floor. While the block remained at rest, at each timestep, $|\dot{u}_{floor,x}| > \mu g$ was checked to detect the onset of sliding. Once sliding was initiated, the response of the rigid block was explicitly solved using standard ODE solvers in MATLAB [2017]. An event locator was used to halt the ODE solver when the relative velocity between the block and floor became zero, in order to determine whether the block stuck to the floor or continued its motion. The peak relative displacements and velocities of the rigid block were obtained for varying coefficients of friction and the median sliding displacement and velocity spectra are shown in Section 6.3. Similar to the sliding component, the pure rocking response of a rigid block was calculated using standard ODE solvers in MATLAB [2017] in order to determine the demands on unanchored components that were slender enough to rock. Although unanchored components have the ability to exhibit a combination of sliding and rocking, the interface

between the floor and the block was assumed to have sufficient friction to avoid sliding of the block prior to or during rocking. Absolute floor accelerations were applied to the rigid block, with equation of motion [Housner, 1963]:

$$\ddot{\theta} = -p^2 \left(\sin(\text{sgn}(\theta)\alpha - \theta) + \frac{\ddot{u}_{floor,x}}{g} \cos(\text{sgn}(\theta)\alpha - \theta) \right) \quad (12)$$

where θ is the rotation of the block, $p = (3g/(4R_{block}))^{1/2}$, and R_{block} and α are shown in Figure 6.1. Similar to the sliding component, an event locator function was used, which detected when the block reached zero rotation during rocking. A coefficient of restitution, e , was used to represent the energy lost during rocking impact. When impact was detected, the post-impact angular velocity was computed by multiplying the pre-impact angular velocity by [Housner, 1963]:

$$e = 1 - \frac{3}{2} \sin^2 \alpha \quad (13)$$

Median rocking spectra were developed at each floor for each system showing the ratio of the peak rotation of the rocking block to the slenderness angle, α . A ratio of 1 represented a block that had overturned. The rocking spectra are shown in Section 6.4.

6.2 Acceleration-Sensitive Anchored Components

6.2.1 Rigid Acceleration-Sensitive Anchored Components

For anchored components that are considered to be rigid (periods of less than 0.06 s [ASCE, 2016]), peak floor accelerations (PFAs) provide a reasonable expectation for anchored component acceleration demands. Referring to Section 6.2.2, the floor spectra were relatively flat in the 0 to 0.06 s period range, although the 3-storey $\beta = 25\%$ CRSBFs did see a gradual increase in pseudo-acceleration in this range likely due to the proximity of

the third mode period of the CRSBF to the rigid-component period range. Therefore, PFAs were deemed an acceptable measure of rigid-anchored component demands for both systems. Figure 6.2 shows a comparison of the median peak floor accelerations (PFAs) at different building heights and earthquake intensities between the two systems. At DBE level for all building heights the PFAs in the BRBF were typically lower than the CRSBFs regardless of the amount of energy dissipation provided. Also notable was that at DBE, the elongation of natural periods in the BRBF does not allow a magnification of the peak ground acceleration over the height of the structure whereas in the CRSBFs the peak floor accelerations were typically magnified compared to the peak ground acceleration. The average of the median PFAs over all floors above ground level is shown in Table 6.1 for each design. The results show that the average of the median PFAs were typically larger than at least 0.64 g in the CRSBFs, but were only around 0.4 to 0.5 g in the BRBFs, over all building heights. When comparing the two CRSBFs, the 3, and 12-storey CRSBFs experienced lower PFAs in the $\beta = 90\%$ CRSBF by 0.09 g and 0.19 g, respectively, but the 6-storey CRSBFs experienced nearly identical average PFAs, with the $\beta = 25\%$ CRSBF having the slightly lower average. Furthermore, the average of the median PFAs in both CRSBFs combined were 32%, 39%, and 32% larger than the peak ground acceleration for the 3, 6, and 12-storey structures, respectively, whereas the average PFAs were 23%, 19%, and 20% lower than the peak ground acceleration for the 3, 6, and 12-storey BRBFs, respectively. However, a comparison of the PFAs between the two systems at $\frac{1}{2}$ and $\frac{1}{4}$ DBE intensities shows differing results. At $\frac{1}{2}$ DBE, although the PFAs were still slightly higher in the CRSBFs, this difference was greatly reduced compared to DBE level. When

observing the $\frac{1}{4}$ DBE intensity, the PFAs were similar between the two systems, with differences of only 0.06 g, -0.01 g (i.e. 6-storey CRSBF PFAs were lower on average than the BRBF), and 0.02 g between the average of 3, 6, and 12-storey CRSBFs to the BRBF median PFAs, respectively. The PFAs in the BRBF also seem to follow a more linear distribution over the height of the buildings, perhaps indicating that the first mode response drives the floor acceleration responses whereas the peak floor accelerations in the CRSBFs seem to be more affected by the higher-mode periods of the frame since the distribution tends to take the shape of the higher-mode periods, particularly the third-mode shape of the CRSBF frame.

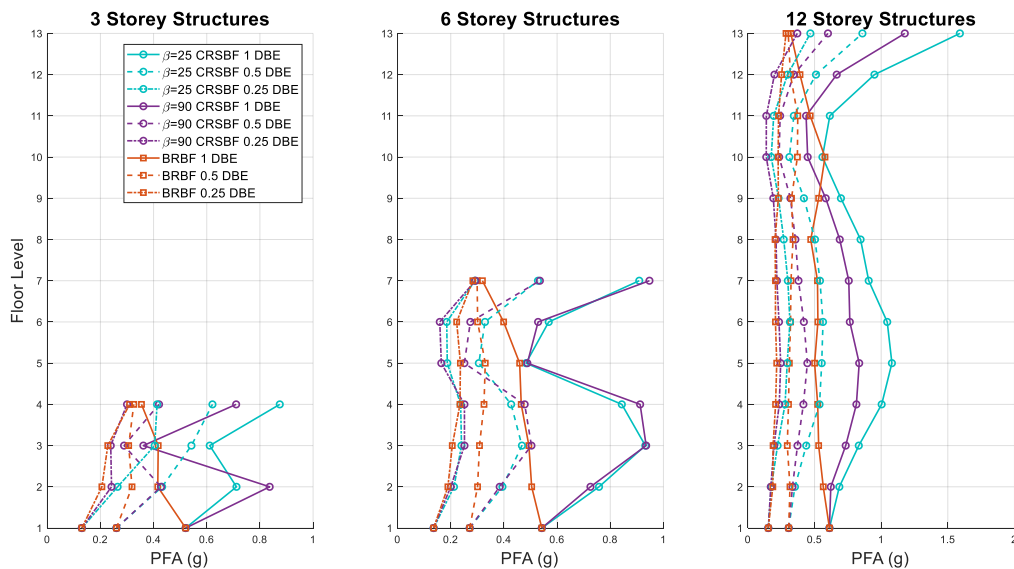


Figure 6.2 CRSBF and BRBF median peak floor accelerations at DBE, 1/2 DBE and 1/4 DBE

Table 6.1 Average median PFA, and pseudo-acceleration at higher-mode rocking periods of CRSBFs, over all floors above ground level

Design	Average DBE PFA above ground level (g)	Mode 2 Rocking Period (s)	Mode 3 Rocking Period (s)	Average DBE Sa (g) at Mode 2	Average DBE Sa (g) at Mode 3
3S- β 25	0.73	0.14	0.10	4.17	3.97
3S- β 90	0.64	0.18	0.13	5.02	2.61
3S-BRBF	0.40	-	-	-	-
6S- β 25	0.75	0.26	0.15	6.05	2.69
6S- β 90	0.76	0.30	0.17	6.14	2.80
6S-BRBF	0.44	-	-	-	-
12S- β 25	0.90	0.53	0.28	6.27	3.94
12S- β 90	0.71	0.60	0.30	3.89	3.08
12S-BRBF	0.49	-	-	-	-

6.2.2 Non-Rigid Acceleration-Sensitive Anchored Components

In order to assess the performance of anchored components that are not considered to be rigid, the median peak pseudo-accelerations for the 3, 6, and 12-storey CRSBF and BRBF structures at DBE and $\frac{1}{4}$ DBE intensity levels are shown in Figure 6.3, Figure 6.4, and Figure 6.5. The vertical lines represent the natural periods of each of the structures, with either the first or second mode period marked on the figures, and the next higher mode periods shown to the left as T_n becomes smaller.

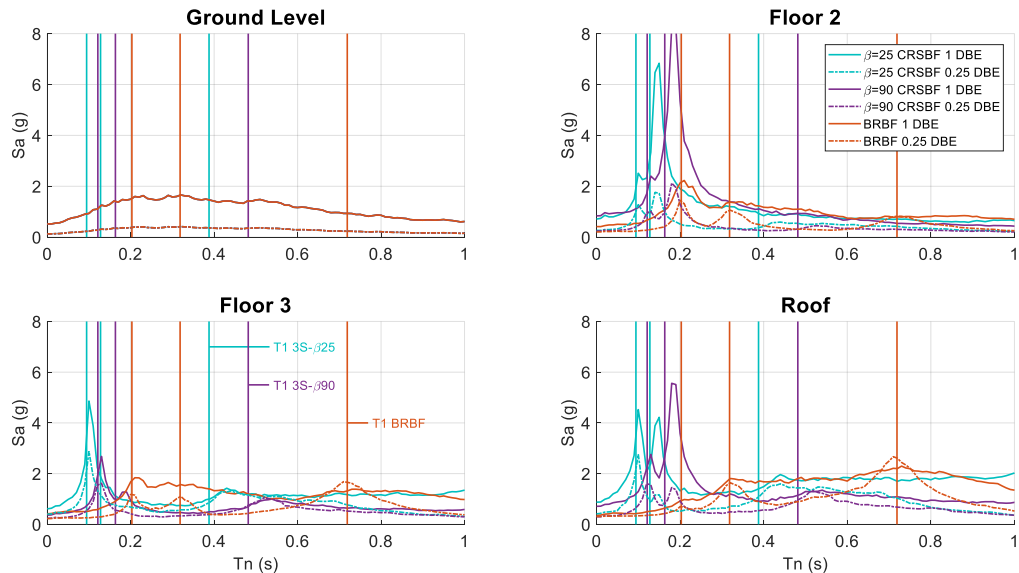


Figure 6.3 3-storey CRSBF and BRBF median pseudo-acceleration floor spectra with $\zeta = 2\%$

A comparison of the 3-storey CRSBF and BRBF floor spectra at DBE level showed that the peaks in pseudo-acceleration in both CRSBFs generally exceeded at least 4 g near the second and third mode periods of the structures, and were larger than those seen in the BRBF, which had peak magnitudes of around 2 g at each floor level. Although the largest magnitudes in floor spectra of the BRBF did occur near the natural periods of the structure, these peaks were much less concentrated than in the CRSBF, as the largest pseudo-accelerations spread out over a wider range of periods. This capping and spreading effect on the pseudo-accelerations is attributed to the elongation of periods in the BRBF as the BRB cores experienced significant yielding at DBE level. Because of this spreading effect, as the anchored component period became larger than the second-mode period of the CRSBFs, there was a crossover point where the pseudo-accelerations between the CRSBFs and BRBF became either similar or larger in the BRBF. Also notable was that at periods greater than 1 s (not shown on the floor spectra for clarity but can be viewed in Appendix

B) the pseudo-accelerations once again became higher in the $\beta = 25\%$ CRSBF than the BRBF, with the largest difference being about 1.25 g occurring at a natural period of 1.25 s. These observations are notable for the performance of more flexible nonstructural components, or vibration isolated components which can have natural periods of greater than 1 s. However, this crossover point may be past the relevant range of periods for the majority of anchored components, as even the most flexible anchored components are estimated to have natural periods upwards of 0.13 s for mechanical equipment, 0.3 s for electrical equipment cabinets, and 0.1 s to 0.2 s for a wide range of other electrical components [ASCE, 2016].

Another observation that may be of interest is the location of the peaks in CRSBF floor spectra compared to the locations of the modes of the CRSBF. At almost every floor level the floor spectra peaks are located not exactly at, but slightly past the higher-mode periods of the CRSBF. Upon further inspection, it was determined that the peaks actually coincided with the instantaneous natural periods of the CRSBF during the rocking phase, which are calculated using the elastic model of the frame while rocking (see Section 2.2 and shown in Table 6.1), rather than the grounded phase. Although these periods are very close to one another, because the boundary conditions of the frame change from being grounded to anchored at only one toe, the periods increase slightly during the rocking phase. For example, the 3-storey $\beta = 25\%$ CRSBF the grounded second- and third-mode periods were 0.128 s and 0.094 s, whereas the second- and third-mode periods obtained from the elastic model of the frame during rocking used for the capacity design procedure were 0.141 s and 0.104 s, respectively.

The average peaks in median pseudo-acceleration over all floors above ground level are shown in Table 6.1 at the higher-mode rocking periods for each CRSBF design. The peak BRBF pseudo-accelerations were omitted from this table as they did not necessarily occur at the higher-mode periods, as shown in the floor spectra for each building height.

The comparison of the performance of acceleration-sensitive anchored components showed a change as the earthquake intensity was reduced to 1/4 of the DBE intensity. In the CRSBFs, the large spikes in pseudo-acceleration near the second- and third-mode periods of the CRSBF saw a significant reduction. On average, for both CRSBFs combined, the peaks were reduced by 72% and 44% at modes two and three, respectively. Although a reduction in pseudo-accelerations was noticeable in the BRBF, the reduction was not as significant (20% and 38% at modes two and three, respectively). In fact, the distribution of the BRBF floor spectra at 1/4 DBE began to match the trends of the CRSBF, with more defined peaks in spectra at the periods of the structure. At the fundamental mode of the 3-storey BRBF, the median floor spectra on average were actually 0.26 g larger at the 1/4 DBE intensity level than at DBE. Referring to the hysteretic response of the 1st storey BRB core for a ground motion of median drift performance in Figure 5.1, at 1/4 DBE the BRBF experienced minimal yielding of the BRB cores and was not relieved from vibrating in its elastic modes for the majority ground motion (similar to the CRSBFs). This limited the spreading and capping effect seen at DBE level. This was a common trend in the floor spectra, as the structural benefit of maintaining an elastic response of the CRSBF frame members resulted in higher magnitudes in floor spectra because the frame was allowed to vibrate consistently at its original higher-mode periods; an observation that was reinforced

by the results of the BRBF at $\frac{1}{4}$ DBE when the frame experienced minimal yielding. The result was a much more similar comparison of the peak magnitudes in floor spectra between the CRSBFs and the BRBF structure. However, due to the longer fundamental period of the designed BRBF structure, the CRSBFs experienced their peaks in floor spectra at shorter periods, which may dominate the range of periods for most anchored components.

The floor spectra for the 6 and 12-storey structures in Figure 6.4 and Figure 6.5 showed similar results and trends to the 3-storey comparison, where the vibration of the CRSBF in its second and third modes caused significant peaks in the floor spectra. For the 6-storey CRSBFs the average peaks in median pseudo-acceleration were 6.05 g and 2.69 g at the second and third modes of the $\beta = 25\%$ CRSBF design, and 6.14 g and 2.80 g at the second and third modes of the $\beta = 90\%$ CRSBF, respectively, compared to the peak median pseudo-acceleration magnitudes in the 6-storey BRBF that were around 2 g at DBE level. As the earthquake intensity was reduced to $\frac{1}{4}$ DBE, the magnitudes of the floor spectra were relatively similar between the CRSBF and BRBF structures, with the exception of some floors where the peaks of the CRSBF floor spectra were still slightly larger. Again, because the CRSBF had shorter fundamental periods than the BRBF structure the location of the peaks in pseudo-acceleration at the higher modes (particularly the second mode) may be closer to the range of periods for most anchored components. Also similar to the 3-storey structures was the observation that as the natural period extended past the second-mode periods of the CRSBFs (into the range of periods for vibration isolated components), the magnitudes in floor spectra at both DBE and $\frac{1}{4}$ DBE levels between the two systems were

either comparable, or at times for the 6-storey structure even slightly higher in the BRBF structure.

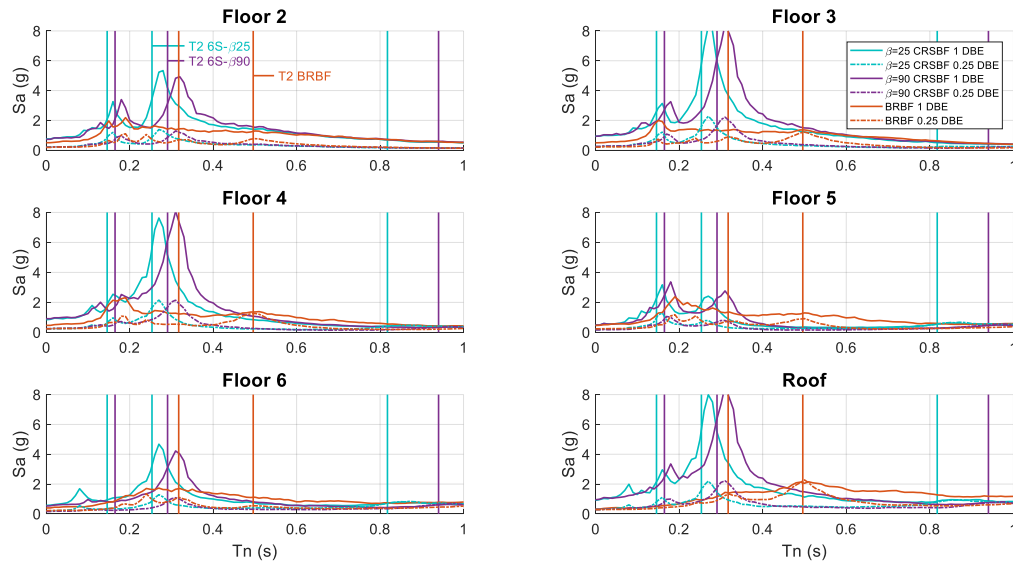


Figure 6.4 6-storey CRSBF and BRBF median pseudo-acceleration floor spectra with $\zeta = 2\%$

At the higher-mode periods of the 12-storey CRSBFs, the peaks in pseudo-acceleration were significantly larger than the peaks seen in the BRBF floor spectra. On average, the peaks in median pseudo-acceleration were 6.27 g and 3.94 g at the second and third modes of the $\beta = 25\%$ CRSBF design, and 3.89 g and 3.08 g at the second and third modes of the $\beta = 90\%$ CRSBF, respectively, compared to peak pseudo-acceleration magnitudes that were around 2 g in the 12-storey BRBF. As the height of the structure increased, as expected the participation of the higher modes of the CRSBF resulted in even larger differences in floor spectra magnitudes between the two systems compared to the 3-storey structure, with peaks in floor spectra that reached or exceeded about 8 g at multiple levels for both the 6 and 12-storey CRSBFs. Although the peaks occurring at the higher-mode periods of the CRSBF seem to provide some relevance to the concern that “larger member

forces caused by higher-mode vibrations of the CRSBF during rocking may also lead to an increase floor accelerations,” the comparison of the concentration of the floor spectra peaks to the BRBF structure at DBE and ¼ DBE suggest that these peaks were caused by the CRSBFs vibrating in their elastic modes for the entirety of the ground motions, rather than the CRSBF having a significantly larger contribution of the higher modes than the BRBF structure.

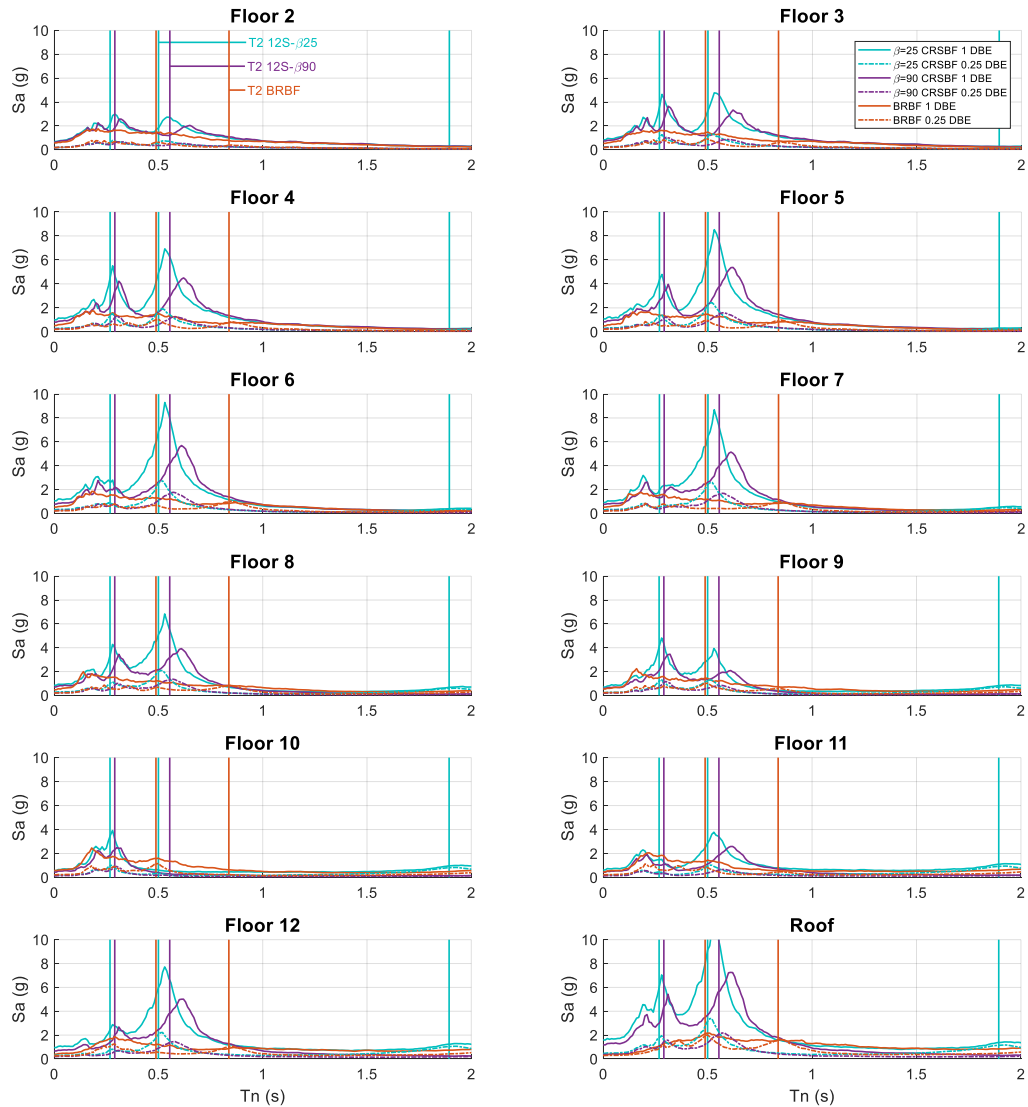


Figure 6.5 12-storey CRSBF and BRBF median pseudo-acceleration floor spectra with $\zeta = 2\%$

Another notable observation was that despite the large differences in supplemental energy dissipation provided to the two CRSBFs at each height, the peaks in pseudo-acceleration were not consistently smaller in the $\beta = 90\%$ CRSBF designs. For the 3 and 12-storey CRSBFs, depending on the stiffness of the capacity designed frame, floor level, and anchored component period, although the peaks were typically slightly smaller for the $\beta = 90\%$ CRSBF designs, the opposite was also the case at other floors and periods. When examining the 6-storey floor spectra, although the locations of the peaks differed, the magnitudes of the peaks were very similar between the $\beta = 25\%$ and $\beta = 90\%$ CRSBF designs. A comparison of the floor spectra for the two different CRSBF base rocking joint designs but having identical capacity designed frames is shown in Section 6.2.3, and provides further insight into the influence of the base rocking joint design and frame stiffness on CRSBF floor spectra performance.

Finally, for all structure heights, the floor spectra suggest that specific attention should be paid to anchored components in CRSBFs considering, in lieu of floor spectra, ASCE permits the use of peak floor accelerations amplified by a component amplification factor, varying from 1.00 to 2.50 for a variety of different nonstructural components [ASCE, 2016], to calculate expected seismic forces acting on the component. If these factors have been chosen based on the general trends of floor spectra in seismic force resisting systems with distributed plasticity, they would likely underestimate the magnitudes of pseudo-acceleration that would be experienced for anchored components in a CRSBF.

6.2.3 Comparison of Floor Spectra in Different CRSBF Designs

With reference to the PFAs and floor spectra in Figure 6.2, Figure 6.3, Figure 6.4, and Figure 6.5 above, it is worth noting that although the CRSBFs designed with more energy dissipation ($\beta = 90\%$) generally had slightly lower PFAs and spectral pseudo-accelerations for the 3 and 12-storey CRSBFs, the differences were not substantial, nor were they the case at every storey level or anchored component natural period. Conversely, the 6-storey CRSBF saw very similar PFAs and peak pseudo-acceleration magnitudes between the two designs. This was a surprising observation considering the large difference in supplemental damping, β , a parameter that is often considered to play an important role in reducing seismic forces and accelerations. Therefore, to further investigate the influence of the base rocking joint and capacity designed frame of the CRSBFs on the floor acceleration performance, nonlinear time-history analyses were also performed on two CRSBFs for each building height with identical base rocking joint designs as the previous designs, but both using the stiffest capacity designed frame (i.e. the $\beta = 25\%$ CRSBF design). Figure 6.6, Figure 6.7, and Figure 6.8 show the resulting floor spectra of the CRSBFs with identical frame members but differing base rocking joint designs, along with the original $\beta = 90\%$ CRSBF floor spectra. The 3 and 12-storey floor spectra results suggest that with an identical frame, CRSBFs with more supplemental energy dissipation reach slightly lower peaks in pseudo-acceleration. However, the differences between the floor spectra for the two different 6-storey base rocking joint designs with identical frame stiffness were nearly negligible. With reference to Table 2.1, the two 6-storey CRSBF base rocking joint designs had very similar effective force reduction factors (R was only about 6% larger in

the $\beta = 90\%$ CRSBF compared to the $\beta = 25\%$ CRSBF), whereas the 3 and 12- storey $\beta = 90\%$ CRSBFs had R factors that were markedly larger than the $\beta = 25\%$ (about 35% and 32% larger for the 3 and 12-storey $\beta = 90\%$ CRSBFs, respectively), meaning that their base rocking moments were lower. This suggests that in terms of the base rocking joint design, the amount of supplemental energy dissipation has a minimal influence on floor spectra magnitudes, particularly in the range of the higher modes of the frame, whereas the rocking moment of the CRSBF does influence the pseudo-accelerations, as CRSBFs that were designed with lower rocking moments had slightly lower magnitudes in floor spectra and peak floor accelerations when considering designs with identical frame stiffness. Although more yielding and therefore more energy dissipation had a spreading and capping effect on the BRBF floor spectra, the energy dissipation provided in the CRSBF is only applied through the friction interface device, which is almost entirely engaged through the uplifting fundamental rocking mode response of the frame, and therefore has a minimal impact on altering the higher modal properties of the frame. Appendix C displays the same floor spectra with natural period range extending to 3 s. Observing the 0.5 s to 1.5 s period range in the floor spectra for the 3-storey CRSBFs with identical frames in Figure C.1 (which might relate to a secant period as the fundamental rocking mode period of the $\beta = 25\%$ CRSBF is 1.68 s) might suggest that more energy dissipation can reduce the floor spectra between the fundamental grounded frame period and the fundamental rocking period. However, the results are less conclusive for the other two structure heights. Furthermore, this period range is likely outside the range of relevant natural periods even for many isolated nonstructural components. These observations further emphasize the

point that for the CRSBF, the frame stiffness, and more so the fact that the frame is able to remain elastic and vibrate in its natural modes for the entire ground motion, were what drove the peaks in floor spectra for the system. The designed base rocking moment also played a small role in the magnitudes of the floor spectra as it altered the amount of time that the CRSBF was in the rocking phase during the ground motion.

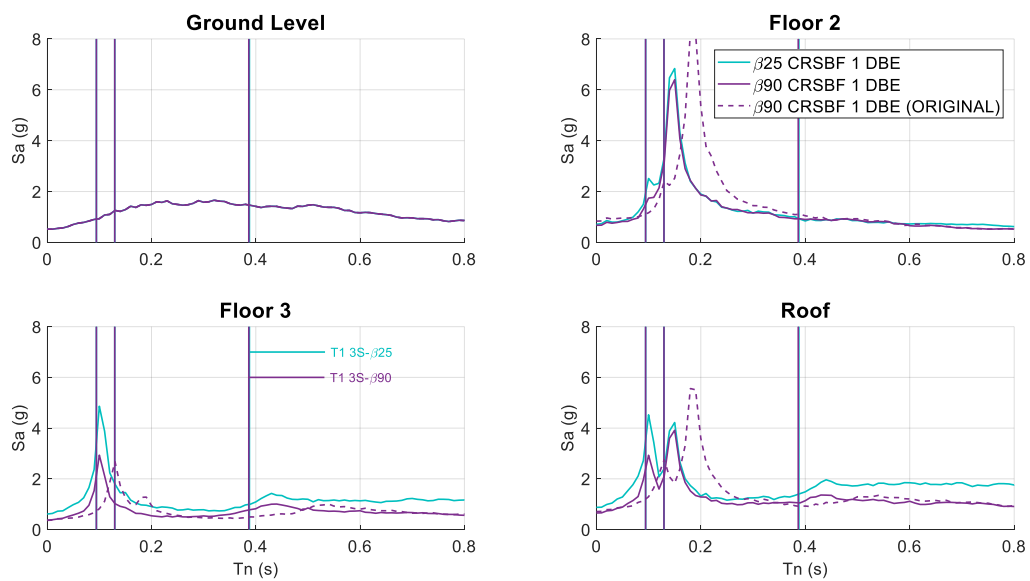


Figure 6.6 3-storey CRSBFs designed with identical frames, median pseudo-acceleration floor spectra with $\zeta = 2\%$

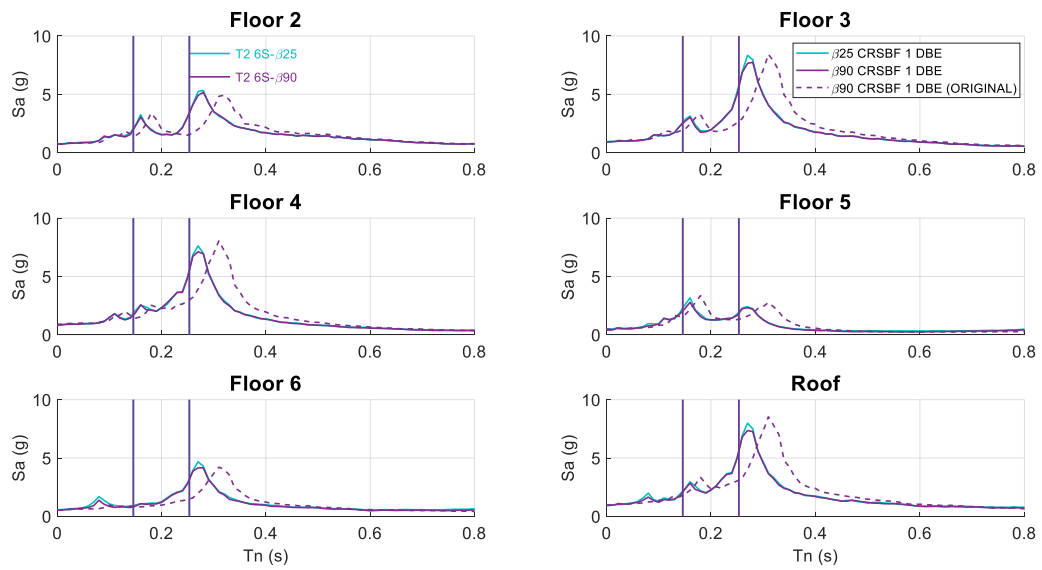


Figure 6.7 6-storey CRSBFs designed with identical frames, median pseudo-acceleration floor spectra with $\zeta = 2\%$

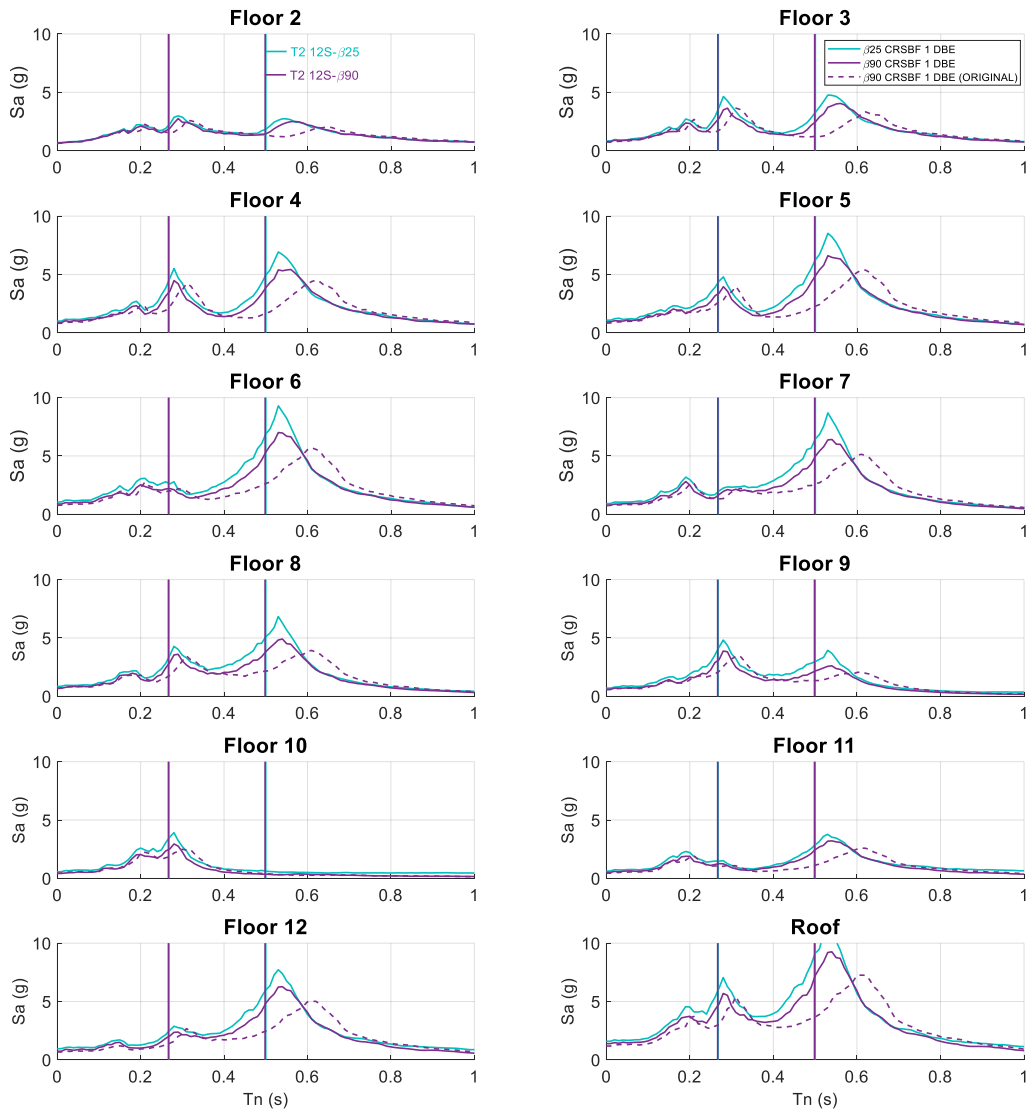


Figure 6.8 12-storey CRSBFs designed with identical frames, median pseudo-acceleration floor spectra with $\zeta = 2\%$

6.3 Unanchored Sliding Components

Sliding spectra that captured the peak sliding displacement and velocity of components with varying μ on each floor were developed, and the median results are shown in Figure 6.9 to Figure 6.14.

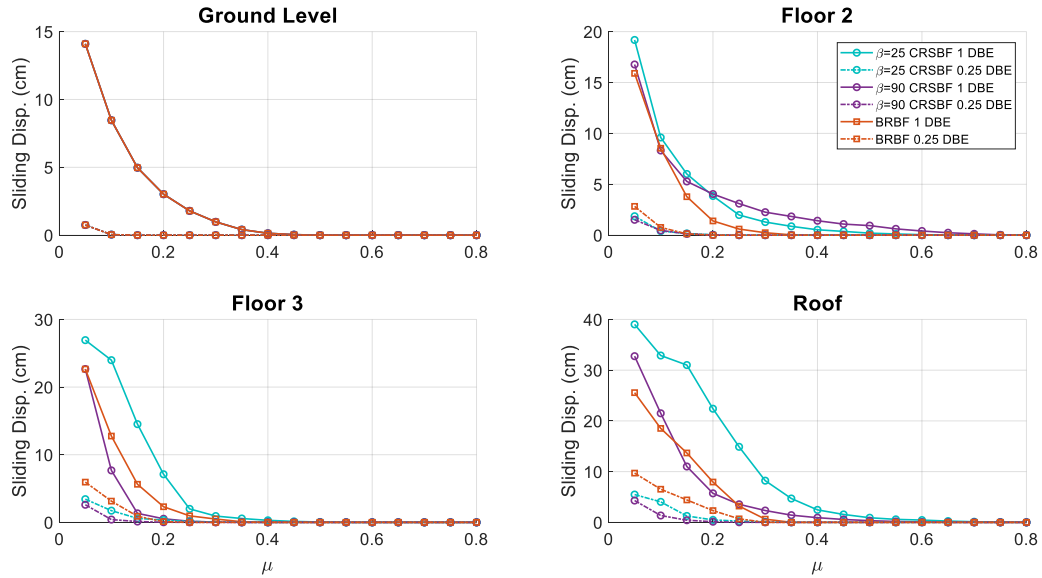


Figure 6.9 3-storey CRSBF and BRBF sliding component median displacement spectra

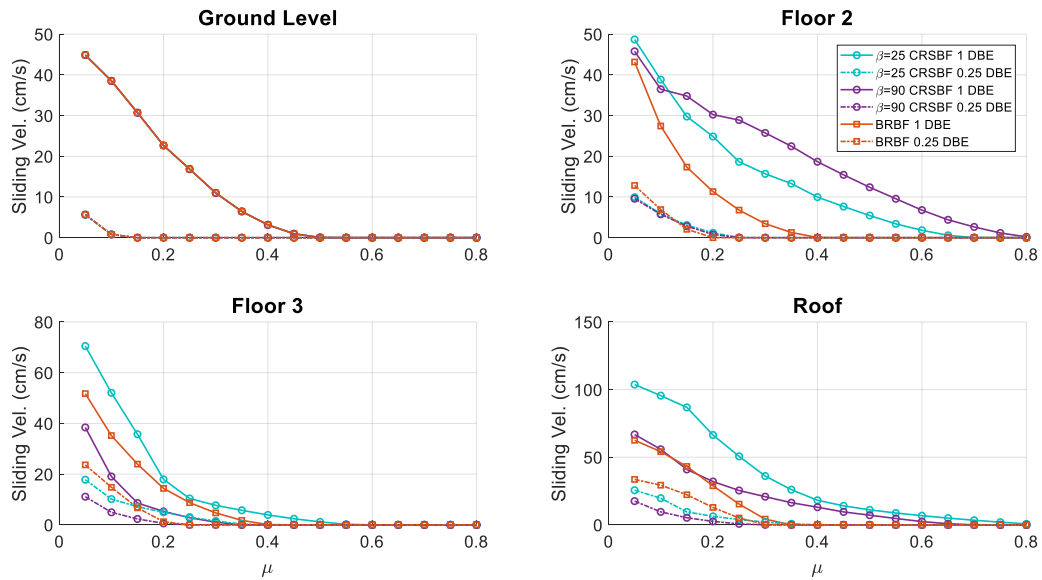


Figure 6.10 3-storey CRSBF and BRBF sliding component median velocity spectra

The 3-storey sliding spectra show that at DBE level the CRSBFs generally experienced larger sliding displacements and velocities than the BRBF structure; the exception being that at some locations and μ values the $\beta = 90\%$ CRSBF experienced lower peak sliding magnitudes than the BRBF structure. For larger values of μ (0.4 to 0.8), the BRBF did not

experience any sliding at median levels, while both CRSBFs experienced sliding with the exception of the $\beta = 90\%$ CRSBF at the third floor. For smaller values of μ (0.05 to 0.35), at all floor levels above the ground floor, the $\beta = 25\%$ CRSBF averaged sliding component displacements and velocities that were about 6.7 cm and 20.6 cm/s larger, respectively, than in the BRBF, while the $\beta = 90\%$ CRSBF only averaged sliding displacements and velocities that were about 0.2 cm and 3.5 cm/s larger than in the BRBF. Although the sliding spectra results seemed to follow the general trend of the PFAs, which can be observed in Figure 6.2 (i.e. BRBF least sliding, followed by $\beta = 90\%$ CRSBF and then $\beta = 25\%$ CRSBF), the differences in peak sliding displacement and velocity were not large relative to the significant differences in PFAs. This was especially the case for the $\beta = 90\%$ CRSBF and both CRSBFs at low values of μ . For example, the average sliding displacement of both CRSBFs combined at the second floor was only 15% larger than the BRBF for $\mu \leq 0.15$, even though the average of the CRSBF PFAs at this level was about 86% larger than the BRBF PFA. This observation can also be seen at the roof level where the average sliding displacement in the $\beta = 90\%$ CRSBF for $\mu \leq 0.35$ was only 11% larger than the BRBF average sliding displacement, despite a PFA that was twice as large. Another notable observation at the second floor was that for $\mu \leq 0.15$ the $\beta = 90\%$ CRSBF had lower sliding displacements than the $\beta = 25\%$ CRSBF even though the PFA was 18% larger in the $\beta = 90\%$ CRSBF. These results suggest that PFAs are not necessarily a strong indicator of peak sliding demands. Also notable was that similar to the acceleration-sensitive anchored component performance, sliding component demands were generally lower for the $\beta = 90\%$ CRSBF than the $\beta = 25\%$ CRSBF.

When the earthquake intensity was reduced to $\frac{1}{4}$ DBE, the sliding displacements and velocities were generally comparable or lower in the CRSBFs compared to the BRBF, even though the PFAs at $\frac{1}{4}$ DBE were slightly larger in the CRSBFs. At all floor levels above the ground, and for $\mu \leq 0.2$, the $\beta = 25\%$ CRSBF and $\beta = 90\%$ CRSBF experienced average sliding displacements that were about 1.4 cm and 2.1 cm less than in the BRBF, respectively. However, although sliding performance at $\frac{1}{4}$ DBE was either similar or generally better in the CRSBFs than the BRBF, the amount of sliding at this intensity was minimal and in general at the median level there was negligible sliding at μ values greater than 0.2, which would govern the majority of sliding components.

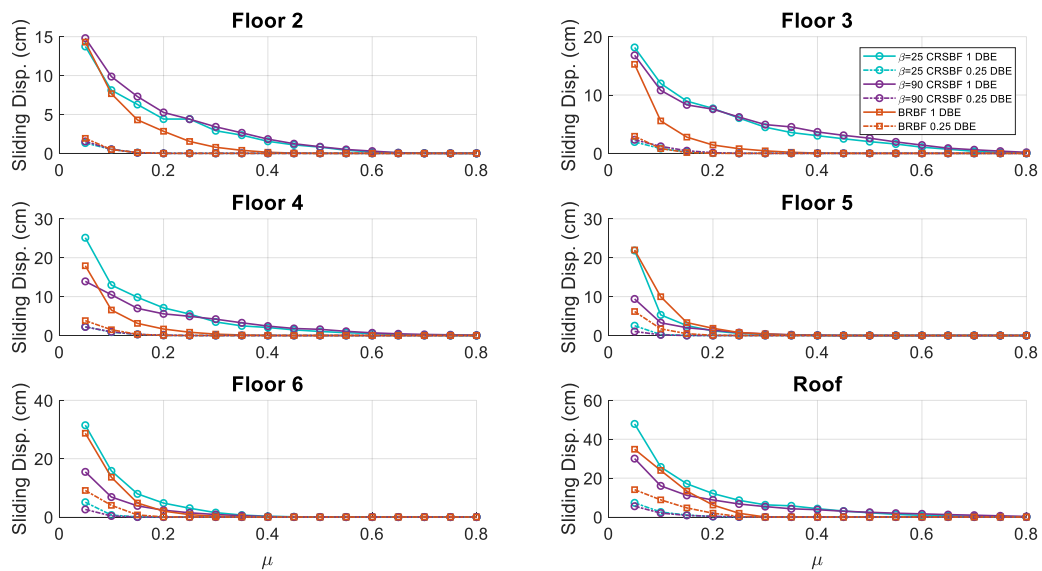


Figure 6.11 6-storey CRSBF and BRBF sliding component median displacement spectra

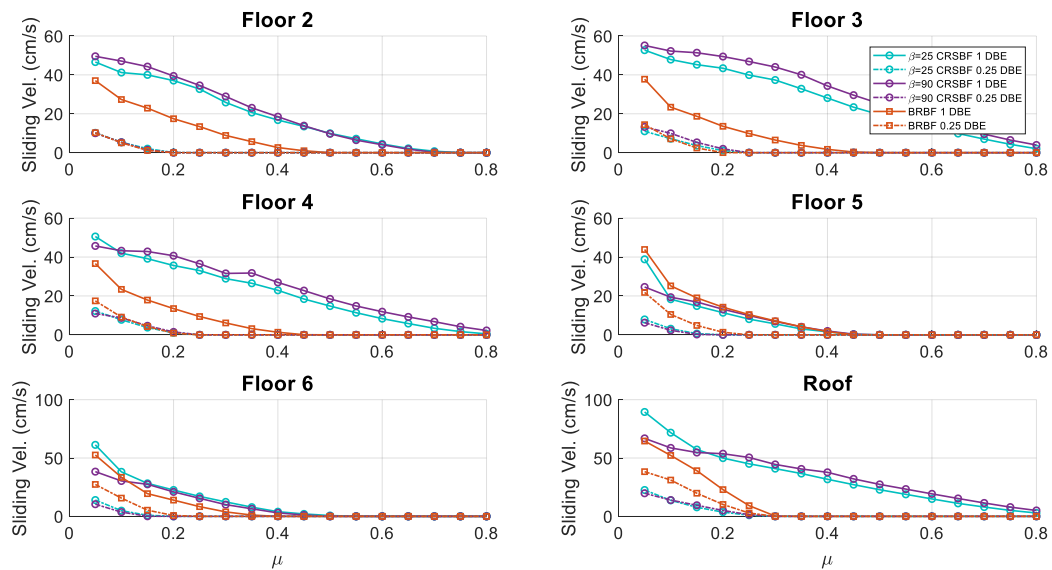


Figure 6.12 6-storey CRSBF and BRBF sliding component median velocity spectra

Figure 6.11 and Figure 6.12 show the median sliding spectra for the 6-storey structures. At DBE level, the 6-storey CRSBFs had higher PFAs than the BRBF at every floor level, but this difference was the most significant at floors three and four and was the smallest at floors five and six. For larger values of μ (0.4 to 0.8), the BRBF did not experience any sliding at median levels, while both CRSBFs experienced some sliding with the exception of floors five and six. For smaller values of μ (0.05 to 0.35), at all floor levels above the ground floor, the $\beta = 25\%$ CRSBF averaged sliding component displacements and velocities that were about 3.3 cm and 15.8 cm/s larger, respectively, than in the BRBF, while the $\beta = 90\%$ CRSBF only averaged sliding displacements and velocities that were about 0.4 cm and 15.6 cm/s larger than in the BRBF. Interestingly, although the average sliding displacements were slightly lower in the $\beta = 90\%$ CRSBF compared to the $\beta = 25\%$ CRSBF, sliding velocities were typically slightly larger in the $\beta = 90\%$ CRSBF, with the exception of very low values of μ . Also noticeable was that the difference in sliding

velocities between the two systems seemed to be more pronounced than the differences in sliding displacement, particularly at floors two to four and the roof level. Considering that the difference in PFAs between the two 6-storey CRSBFs on average was only about 0.007 g, it appears that PFAs are a better indicator of sliding component velocity than sliding displacement. Furthermore, sliding displacements and velocities for larger coefficients of friction generally followed the PFA trend where floors five and six were the two floors where sliding magnitudes were comparable between the CRSBFs and the BRBF, whereas sliding component performance was markedly worse in the CRSBF at other floor levels. However, at floor 5 where the average PFAs in the CRSBFs were only about 6% larger than the BRBF, the average sliding displacement $\mu \leq 0.35$ were 2.3 cm lower in the CRSBFs. This suggests that although sliding demands at DBE were generally higher in the CRSBFs, this was likely due to the fact that the floor acceleration demands were markedly higher in the CRSBFs, but when comparing floor levels with similar acceleration demands, the BRBF system seems to have somewhat larger sliding demands. Past research [Konstantinidis and Makris, 2009; Konstantinidis and Nikfar, 2015; Nikfar and Konstantinidis, 2017] has shown that for analytical pulse excitations, sliding component response correlates better with the so-called *persistence* of the excitation, which is a characteristic length scale of the excitation that is affected linearly by the strength of excitation (PFA) and quadratically by period of the excitation. Under earthquake floor excitation, the response of the sliding block is more nuanced, but it generally increases with PFA and with the period of excitation. Therefore, although it was expected that peak sliding demands would be much larger in the CRSBFs based on the PFAs, the differences were a

bit more moderate, perhaps due to the longer fundamental period of the BRBF structures. Also consistent with the 6-storey structure (compared to the 3-storey structure) was the fact that at very low μ values, although sliding magnitudes were still generally larger in the CRSBFs than the BRBF, the results were more comparable between the two systems, even when the difference in PFA was significant. For example, at the 4th floor for $\mu \leq 0.1$, on average sliding displacements were about 28% larger in the CRSBFs than the BRBF, whereas the PFAs on average were 89% larger in the CRSBFs. This trend also applied to the sliding velocities but not as significantly, as the average sliding velocities in the CRSBFs were about 51% larger for $\mu \leq 0.1$ at the 4th floor, which was closer but still well below the amount that the PFAs in the CRSBFs were larger than the BRBF (89%). This suggests that at very low values of μ , the longer fundamental period of vibration in the BRBF has a more significant impact than PFA relative to larger values of μ . At $\frac{1}{4}$ DBE again the sliding magnitudes were minimal and generally comparable between the two systems.

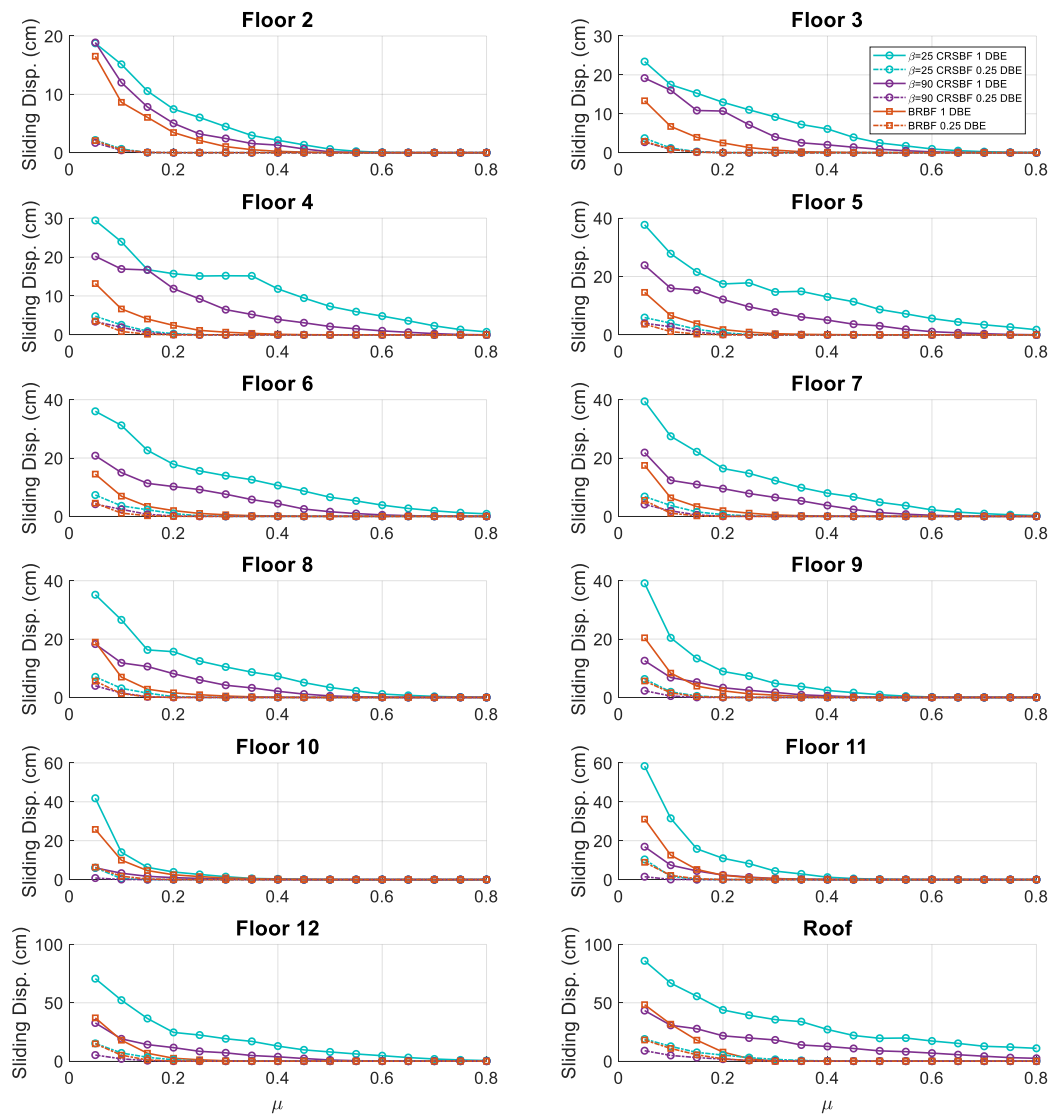


Figure 6.13 12-storey CRSBF and BRBF sliding component median displacement spectra

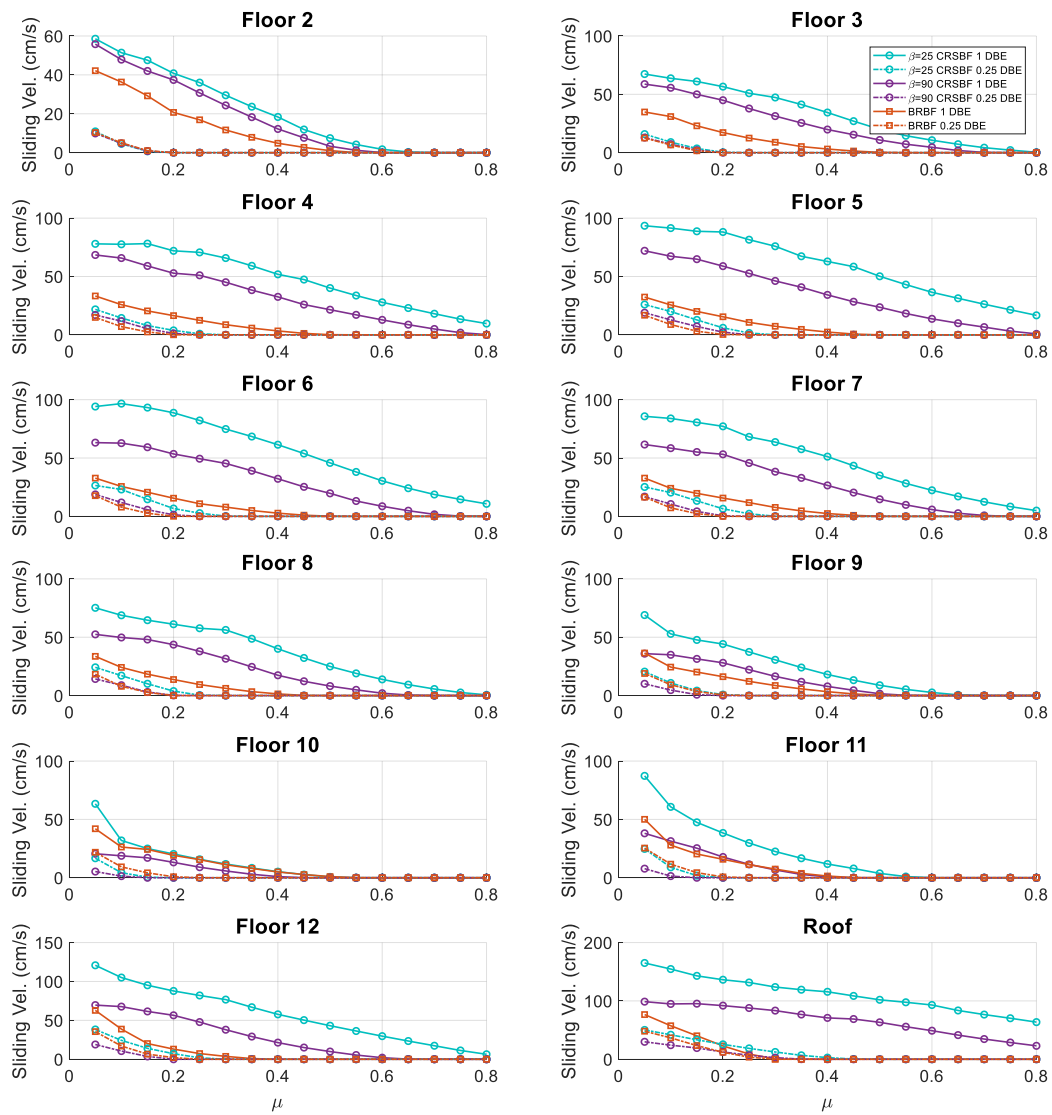


Figure 6.14 12-storey CRSBF and BRBF sliding component median velocity spectra

Figure 6.13 and Figure 6.14 show the median sliding spectra for the 12-storey structures.

In general, more sliding was experienced at DBE level in the CRSBFs which was consistent with the larger magnitudes of PFA and floor spectra in the CRSBF system. For larger values of $\mu \geq 0.35$, the BRBF generally did not experience any sliding at median levels while both CRSBFs experienced some sliding with the exception of floors ten and eleven. For smaller values of μ (0.05 to 0.3), at all floor levels above the ground floor, the $\beta = 25\%$ CRSBF

averaged sliding component displacements and velocities that were 15.5 cm and 48.8 cm/s larger, respectively, than in the BRBF, while the $\beta = 90\%$ CRSBF averaged sliding displacements and velocities that were 4.1 cm and 25.3 cm/s larger than in the BRBF. Of the three building heights, the difference in average sliding displacement and velocity demands between the CRSBFs and BRBFs was the largest for the 12-storey structures. At $\frac{1}{4}$ DBE level, negligible sliding was experienced in all designs for $\mu \geq 0.2$. For $\mu \leq 0.15$, sliding displacement demands were much more similar between the two systems with the $\beta = 25\%$ CRSBF averaging only 1.1 cm more sliding displacement than in the BRBF and the $\beta = 90\%$ CRSBF averaging 1.4 cm less sliding displacement than in the BRBF, although the amount of sliding was small in all cases.

Although observing the PFAs were not a steadfast rule for predicting the amount of sliding displacement and velocity in the CRSBFs and BRBF, they did provide a starting point for which structures would experience the most sliding at any given floor. As discussed above, the *persistence* of the excitation likely brought the comparison of sliding demands closer than would be expected based on large difference in PFAs between the two systems, likely due to the BRBFs having longer fundamental periods than the CRSBFs. Consistent for all three structure heights was that the sliding displacement and velocity performance at DBE level was generally worse in the CRSBFs than in the BRBF structure. When comparing only the CRSBFs, at the 3 and 12-storey building heights, the $\beta = 90\%$ CRSBFs typically had lower median sliding displacements and velocities than the $\beta = 25\%$ CRSBFs. However, for the 6-storey structure, the sliding component performance was very similar when comparing the two CRSBF designs (with the exception of very small values of μ),

which is consistent with the similar PFAs and floor spectra peak magnitudes between the two 6-storey designs. Although the stiffness of the frame and the elastic vibrations of the frame in its natural modes are likely the main influencers of nonstructural component performance in CRSBFs, the results from the sliding component analysis reinforced the observation that, in terms of the base rocking joint design, the R value of the CRSBFs seems to have an influence on nonstructural component demands, where designs with a lower rocking moment and more flexible frame typically experienced lower floor accelerations, sliding displacements, and sliding velocities.

6.4 Unanchored Rocking Components

Median rocking spectra were generated for blocks with three different slenderness angles: 10° , 15° , and 20° , at block sizes ranging from $R_{block} = 0.2$ m to 2.0 m. As previously mentioned, the results show block rotation, θ , as a ratio of the slenderness angle of the block, α , with a ratio of 1 representing a block that has overturned. The rocking spectra for the 3, 6, and 12-storey structures are shown in Figure 6.15, Figure 6.16, and Figure 6.17.

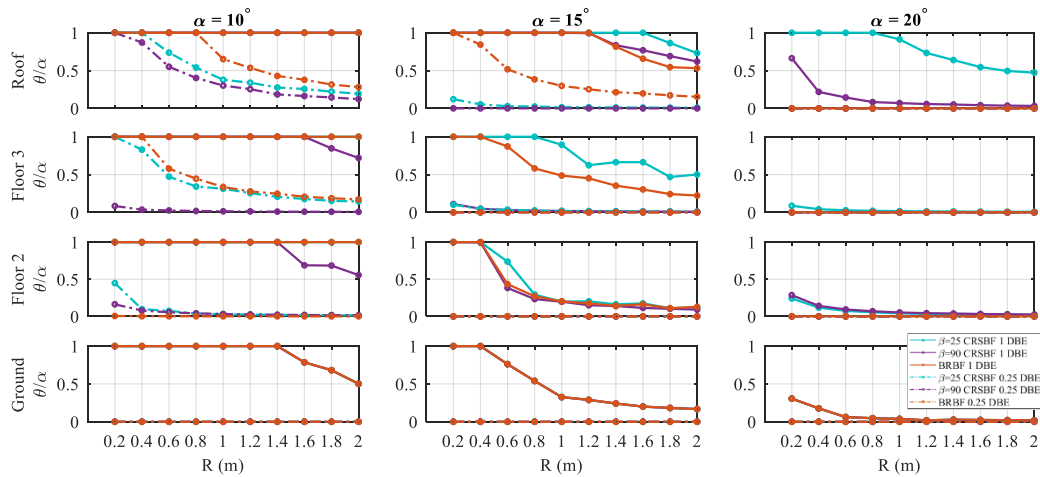


Figure 6.15 3-Storey CRSBF and BRBF rocking component median rocking rotation spectra

Figure 6.15 shows that at DBE level the most slender block ($\alpha = 10^\circ$) overturned for almost all block sizes, in both of the 3-storey structural systems, except for $R_{block} \geq 1.6$ m in the $\beta = 90\%$ CRSBF. For blocks with slenderness of $\alpha = 15^\circ$, the rocking spectra showed very similar performance between the two systems at the second floor, which was surprising considering the CRSBF PFAs were on average 86% larger than the BRBF PFA at this floor. At the third floor, the $\beta = 90\%$ CRSBF experienced the least amount of rocking, with no block exceeding a normalized rotation of 0.11 of $\alpha = 15^\circ$, followed by the BRBF, which experienced overturning at blocks smaller than $R_{block} = 0.6$ m and an average normalized rotation of 0.38 of α for blocks larger than $R_{block} = 0.6$ m, and then finally the $\beta = 25\%$ CRSBF had the largest rotations, experiencing overturning for blocks smaller than $R_{block} = 1$ m and larger rotations than both other designs for larger blocks. The stockiest block ($\alpha = 20^\circ$) experienced the least amount of rocking, with only the $\beta = 25\%$ CRSBF showing blocks overturning at median levels for blocks less than $R_{block} = 1$ m in size and only at the roof level. Also notable was that the rocking spectra for the stockiest block better represented the PFA distribution between the three designs, where in this case the rocking block in the BRBF structure experienced the less rocking than the CRSBFs at the second floor and roof levels where the average PFAs were 86% and 124% larger in the CRSBFs, respectively, and minimal rocking was experienced at the third floor not just in the BRBF but in the CRSBFs as well, where PFAs were the smallest of any level (above the ground) in the CRSBFs. With regards to the two other slenderness angles, at DBE level the $\beta = 90\%$ CRSBF generally had better performance of rocking components than the BRBF, and the $\beta = 25\%$ CRSBF experienced comparable or only slightly worse rocking component

performance, a surprising result considering the disparity in acceleration-sensitive attached component performance between the two systems. These observations suggest that, similar to sliding component displacements, PFA may not be the best indicator of rocking component performance, with the possible exception of stockier rocking components. At ¼ DBE level, for almost all rocking component slenderness angles and sizes, rocking was negligible at all floors. The exception was for rocking components at some floor levels for $\alpha = 10^\circ$, where some of the smallest block sizes experienced overturning, with better performance in the CRSBFs than in the BRBF.

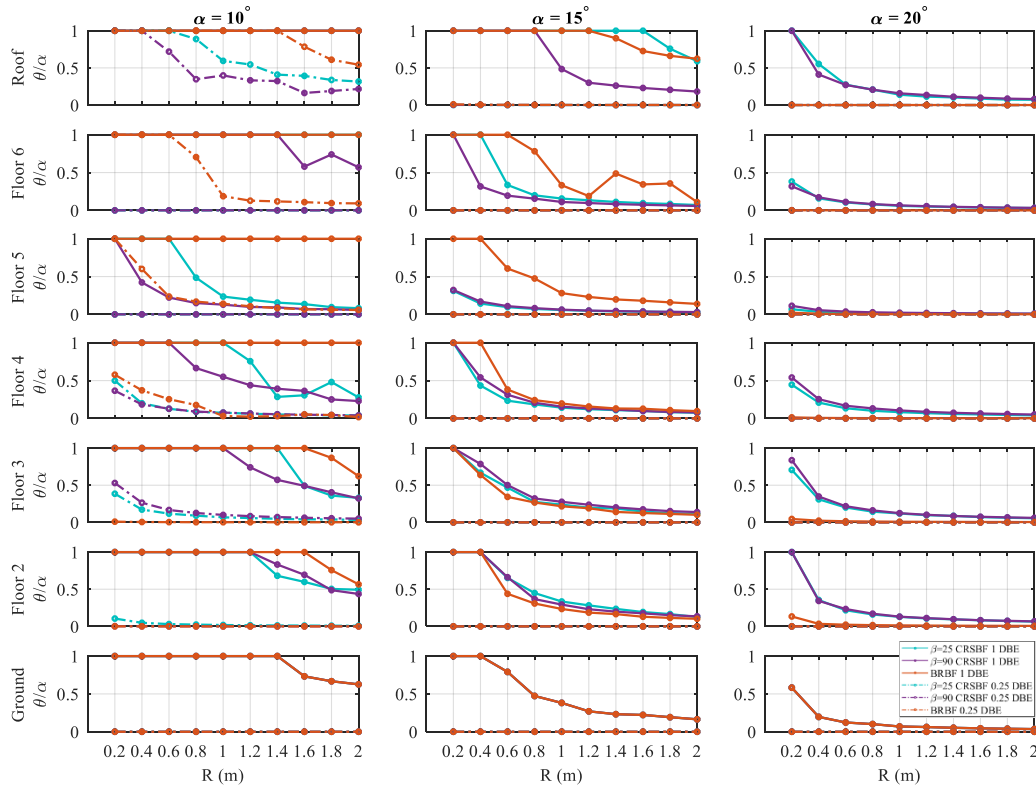


Figure 6.16 6-storey CRSBF and BRBF rocking component median rocking rotation spectra

The median rocking spectra for the 6-storey structures are shown in Figure 6.16. Similar to the 3-storey structure, the most slender block overturned frequently in the 6-storey structure

at the DBE level. Although the PFA at all floor levels was larger in the CRSBFs than in the BRBF, the $\alpha = 10^\circ$ DBE level median rocking spectra show that rocking component performance in the CRSBFs was generally better than the performance in the BRBF, especially at floors two to five where overturning was experienced in the CRSBFs for blocks smaller than around $R_{block} = 1.2$ m, whereas the BRBF experienced overturning at all block sizes below $R_{block} = 1.8$ m. For the $\alpha = 15^\circ$ block, from floors two to four the rocking component performance was similar between the CRSBFs and the BRBF, where only blocks smaller than $R_{block} = 0.6$ m overturned. At these floors, for blocks of $R_{block} = 0.8$ m and larger, block rotations were similar between the CRSBFs and BRBF. At floors five and six the CRSBFs performed better than the BRBF, with a median normalized block rotation for blocks $R_{block} \geq 0.8$ m of about 0.08 in the CRSBFs and 0.3 in the BRBF. Rocking components also overturned more frequently in the BRBFs at these floors at block sizes smaller than $R_{block} = 0.8$ m. These storeys had the smallest discrepancy in PFAs between the CRSBFs and BRBF, but still the PFAs were higher in the CRSBFs than the BRBF at these floors. For block slenderness of $\alpha = 20^\circ$, similar to the 3-storey structure the performance of the rocking components at the DBE level was better in the BRBF, which experienced almost no rocking rotations. Although, overturning was only seen in the CRSBFs at the second floor and roof levels for the $R_{block} = 0.2$ m block, and the average normalized rocking rotation in the $\beta = 25\%$ CRSBF and $\beta = 90\%$ CRSBF for $R_{block} \geq 0.4$ m was only 0.07 and 0.08, respectively. As was the case with the 3-storey structure, the CRSBF rocking component performance was either similar to or better than the BRBF performance for slenderness angles of $\alpha = 10^\circ$ and $\alpha = 15^\circ$ and was slightly worse than the

BRBF rocking component performance for $\alpha = 20^\circ$. Also notable was the fact that in the 3-storey CRSBFs, the $\beta = 90\%$ CRSBF performed better than or similar to the $\beta = 25\%$ CRSBF, whereas in the 6-storey structure the $\beta = 25\%$ CRSBF and $\beta = 90\%$ CRSBF rocking component performance was very similar. This was expected considering the floor acceleration performance of both CRSBFs was similar for the 6-storey structure. At $\frac{1}{4}$ DBE intensity for both systems, the median responses of the $\alpha = 15^\circ$ and $\alpha = 20^\circ$ rocking components experienced no rocking. For the $\alpha = 10^\circ$ rocking component, the CRSBFs generally showed comparable and sometimes better rocking component performance than the BRBF.

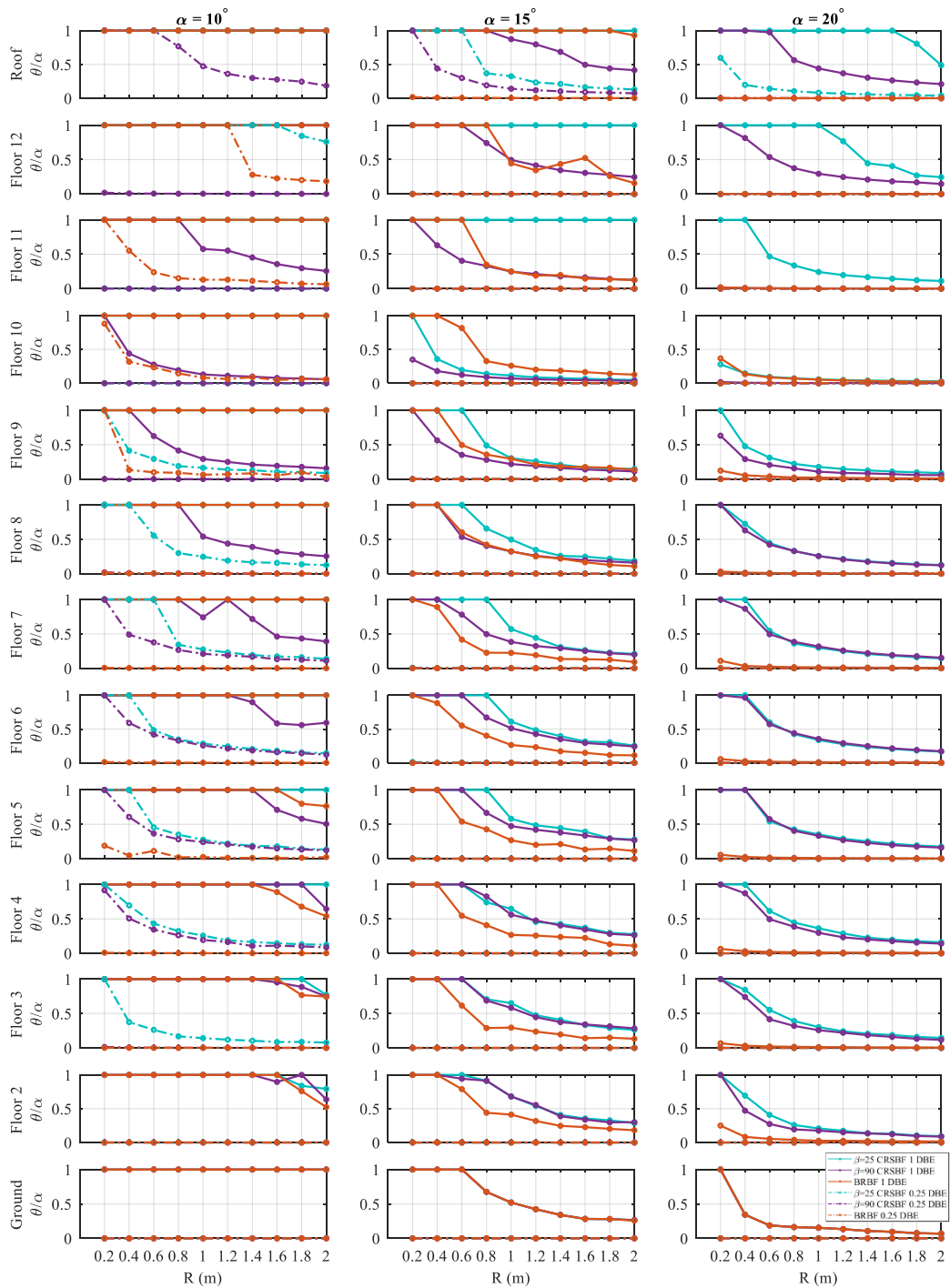


Figure 6.17 12-storey CRSBF and BRBF rocking component median rocking rotation spectra

The median rocking spectra for the 12-storey structures are shown in Figure 6.17. Similar to the 3 and 6-storey structures, the $\alpha = 10^\circ$ rocking components experienced overturning at the majority of floors for the majority of block sizes at DBE intensity, with the exception of the $\beta = 90\%$ CRSBF where some of the rocking components larger than $R_{block} = 1.2$ m did not experience overturning from floors 5 to 11. The $\alpha = 15^\circ$ rocking components experienced better performance in the BRBF than the CRSBFs from floors two to seven where the differences in PFA between the two systems was the largest. At these floors rocking components generally began overturning at sizes less than $R_{block} = 0.6$ m in the BRBF and $R_{block} = 0.8$ m in the CRSBFs. However, once the size of the rocking component exceeded $R_{block} = 0.8$ m, the components generally did not overturn in either system. From floors two to seven, for block sizes larger than or equal to $R_{block} = 1.0$ m, the average normalized rotations in the $\beta = 25\%$ CRSBF, $\beta = 90\%$ CRSBF and BRBF were 0.4, 0.37, and 0.19, respectively. At floors seven to eleven where the PFAs were more comparable, for the $\alpha = 15^\circ$ rocking component, rocking demands were generally comparable or better in the $\beta = 90\%$ CRSBF than the BRBF, and slightly worse in the $\beta = 25\%$ CRSBF. As a comparison between PFA and rocking demands, at floor ten where the $\beta = 25\%$ and $\beta = 90\%$ CRSBF PFAs were 97% and 78% of the BRBF PFA, respectively, the rocking component performance was markedly better in both the $\beta = 25\%$ and $\beta = 90\%$ CRSBF, with average block rotations for all block sizes of 21%, 10% of α , respectively, compared to an average rotation of 42% of α in the BRBF. Finally, for the $\alpha = 20^\circ$ rocking component, similar to the 3 and 6 storey structures, negligible rocking was experienced in the BRBF whereas the CRSBFs experienced a larger amount of rocking and even overturning for the

smallest sized blocks at some floor levels, especially in the $\beta = 25\%$ CRSBF at the higher floors. Again, PFAs were a better indicator for rocking component performance for the stockiest block. This is evident again at the 10th floor where PFAs were very similar between the $\beta = 25\%$ CRSBF and BRBF and so too were the magnitudes of the rocking spectra. At $\frac{1}{4}$ DBE level, similar to the 3 and 6-storey structures, both systems experienced negligible rocking response for the $\alpha = 15^\circ$ and $\alpha = 20^\circ$ rocking components. For the $\alpha = 10^\circ$ rocking components, at lower floor levels where the $\frac{1}{4}$ DBE PFAs were slightly larger in the CRSBFs than the BRBF, the rocking component performance in the CRSBFs were also worse, with some smaller sized rocking components overturning at a few of the floor levels. At floors 10 and 11 where $\frac{1}{4}$ DBE PFAs were slightly higher in the BRBF, the BRBF rocking component demands were higher than in the CRSBFs. This observation was in contrast to the observations at the higher DBE level intensity where PFA performance did not seem to predict the rocking component performance of the slender $\alpha = 10^\circ$ rocking components.

In summary, in contrast to the acceleration-sensitive anchored component and sliding component performance results, the demands on rocking components between the CRSBFs and BRBF were much more comparable. For rocking components with slenderness angles of $\alpha = 10^\circ$ and $\alpha = 15^\circ$, the CRSBFs generally had similar and sometimes better rocking component performance compared to the BRBF, whereas the stockiest rocking component ($\alpha = 20^\circ$) experienced better performance in the BRBF. Overall, a comparison of the three different building heights showed that while the trends in rocking spectra comparing the varying designs and block slenderness angles were typically similar across all three

building heights, the 12-storey structures saw overturning of rocking components begin at slightly larger block sizes, followed by the 3-storey structures and finally the 6-storey structures. When comparing the two CRSBFs, rocking component performance in the $\beta = 90\%$ CRSBF was typically similar to, or better than the $\beta = 25\%$ CRSBF for the 3-storey and 12-storey structures, which was expected based on the relative performance of floor accelerations between the two designs. However, for the 6-storey CRSBFs, rocking component performance was very similar between the two designs which aligns with the previous observations of anchored and sliding component performance. The similar rocking component performance in the 6-storey CRSBFs again suggests that the amount of supplemental energy dissipation provided in the base rocking joint design does not have a significant impact on nonstructural component performance, whereas the designed rocking moment and stiffness of the frame likely play a larger role. This suggests that CRSBFs designed with the smallest base rocking moment and most flexible frame (the $\beta = 90\%$ CRSBFs), while still meeting their target drift and structural member performance, seem to experience lower demands on acceleration-sensitive nonstructural components.

6.5 Effect of CRSBF Grounding on Nonstructural Component Performance

As mentioned in Section 1.1, one concern for nonstructural component performance in CRSBFs is whether the CRSBF hysteretic response transferring from a low lateral stiffness, during rocking, to a high lateral stiffness, after grounding, can lead to a spike in the lateral floor accelerations or sliding/rocking component response. To study this concern, the responses of the various types of anchored and unanchored nonstructural components are plotted alongside the column uplift history of the CRSBFs. Figure 6.18 shows the floor

acceleration response and pseudo-acceleration response for anchored components with periods of 0.15 s and 0.44 s in the 3-storey $\beta = 25\%$ CRSBF during the Superstition Hills ground motion (Poe Road recording station). The two anchored component natural periods coincided with local peaks in the floor spectra near the first- and second-mode periods of the CRSBF. This ground motion was just under the 84th percentile in terms of PFA at the roof level and was chosen in order to assess a ground motion with significant floor accelerations while also having clearly defined cycles of CRSBF grounding. Vertical lines are plotted alongside the responses to denote a grounding event of the rocking frame. A positive value of column uplift coincides with the CRSBF displacing in the positive lateral direction.

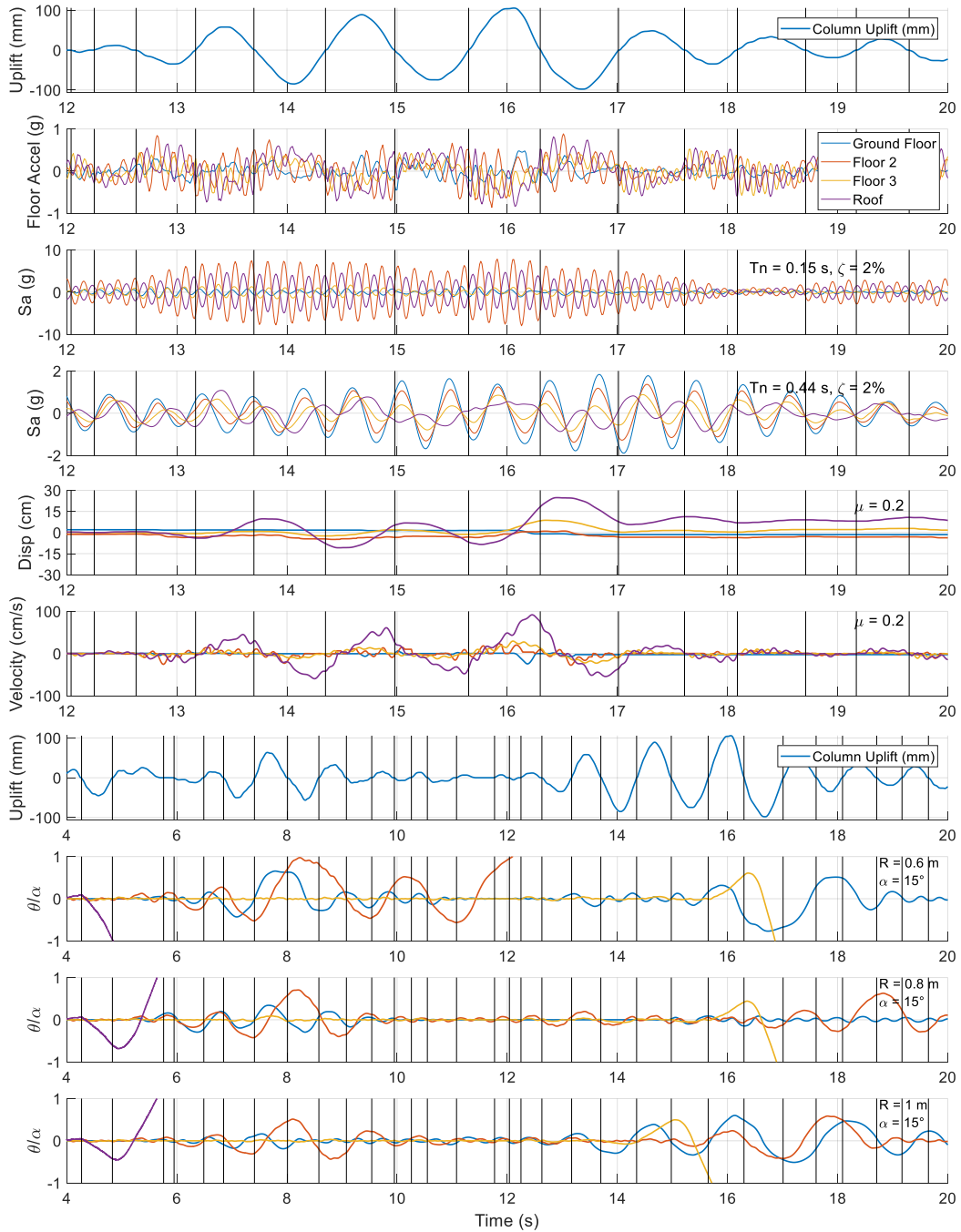


Figure 6.18 3-storey $\beta=25\%$ CRSBF column uplift, floor acceleration, attached component, sliding component and rocking component time-history responses during the Superstition Hills, Poe Road ground motion

The responses show that the floor accelerations and pseudo-accelerations of the anchored components did not experience any significant spikes following CRSBF grounding, but

rather exhibited similar magnitudes and frequencies before and after grounding. Figure 6.18 also shows the effect of frame grounding on a sliding component with $\mu = 0.2$, a friction coefficient that was deemed low enough to examine the effect of CRSBF grounding on a sliding component with a marked amount of sliding. Again, at each floor level there did not seem to be any significant changes in either the displacement or velocity response of the sliding component after grounding of the frame. Finally, the rotations of three rocking components of slenderness $\alpha = 15^\circ$ varying in size from $R_{block} = 0.6$ m to $R_{block} = 1$ m are also plotted alongside CRSBF grounding for a wider time range in Figure 6.18. For the rocking components that did not overturn, the results did not show any notable changes in the magnitudes or rate of increase of the rocking rotations immediately after CRSBF grounding compared to the general magnitude and frequency of the rotation response prior to grounding.

Chapter: 7 Conclusions and Recommendations

7.1 Conclusions

As the field of earthquake engineering pushes towards developing more resilient seismic force resisting systems, Controlled Rocking Steel Braced Frames (CRSBFs) have gained increased attention as a potential high-performance structural solution to limit structural damage and residual drifts. However, the performance of nonstructural components can also have a significant impact on building occupant safety and economic losses experienced during a seismic event. Because the plastic mechanism of a CRSBF is uplift and rocking of the frame rather than distributed plasticity of the structural members, concerns have been raised about the performance of nonstructural components in the system being influenced by effects that are not experienced in a conventional seismic force resisting system, namely, significant higher-mode vibrations during rocking leading to increased floor acceleration responses, and the potential for the transition from low to high lateral stiffness as the frame transfers from rocking to grounding to cause a lateral jerking effect that could adversely impact the response of anchored and unanchored components. While previous studies have analyzed the performance of nonstructural components in CRSBFs to some extent, they have been limited in the number of storeys, base rocking joint design variations, and nonstructural components considered. Furthermore, the validity of the aforementioned concerns for nonstructural components specific to CRSBFs have not been explored. This study compared the seismic performance of anchored and unanchored nonstructural components in CRSBFs with differing base rocking joint designs, to the performance in

BRBF structures, while also exploring what the main influencing factors are for nonstructural component demands in CRSBFs.

For building heights of 3, 6, and 12-storeys, nonlinear time-history analyses were conducted on two CRSBFs with large differences in supplemental energy dissipation ($\beta = 25\%$ and $\beta = 90\%$), and one Buckling Restrained Braced Frame (BRBF). Because nonstructural components can be displacement-sensitive or acceleration-sensitive, the effective force reduction factor of the designs was iterated until the median peak interstorey drifts were within 5% of the target design interstorey drift of 1.5%, thus suggesting a similar performance of displacement-sensitive components. The structural results showed that the CRSBF frame members were capacity protected from elastic buckling at the 84th percentile level with the exception of the 12-storey $\beta = 25\%$, though this result was not expected to affect the analysis of nonstructural components at a median level. The residual drift performance was much better in the CRSBFs, which self-centred after the design basis earthquake (DBE) level events, whereas the BRBFs experienced median residual drifts of around 0.35% to 0.4%, with many ground motions causing residual drifts greater than 0.5%.

The performance of acceleration-sensitive anchored nonstructural components of varying natural periods was assessed using elastic floor spectra. Considering rigid anchored components (periods of less than 0.06 s), the peak floor accelerations showed that at DBE level the CRSBFs experienced an amplification of the peak ground acceleration at most floors, whereas the BRBF peak floor accelerations were lower than the peak ground acceleration. For all building heights, the distribution of peak floor accelerations generally

followed the shape of the third mode in the CRSBFs but followed the shape of the first mode in the BRBFs. At $\frac{1}{2}$ DBE intensity, the peak floor accelerations were more comparable but still slightly higher in the CRSBF than in the BRBF at most floors, while at $\frac{1}{4}$ DBE the peak floor accelerations were very similar between the two systems and were magnified relative to the peak ground acceleration in both systems. At DBE level, the spectral pseudo-accelerations were larger in the CRSBFs, with peaks forming near the higher-mode periods of the rocking frame, compared to the BRBF floor spectra which saw a capping and spreading over wider ranges of periods due to the elongation of the natural periods of the frame as the braces yielded. The floor spectra magnitudes generally became comparable or larger in the BRBF than the CRSBF at longer periods, relevant for isolated components, but in the range of periods relevant for most anchored components (0 to 0.3 s) the large peaks at the higher-modes of the CRBSF showed that the acceleration-sensitive anchored component performance was markedly worse in the CRSBF across all structure heights at DBE level. As the earthquake intensity was reduced to $\frac{1}{4}$ DBE, the floor spectra magnitudes became much more comparable between the two systems, although, because the CRSBFs were typically stiffer than the BRBFs, the spectral accelerations near the higher-modes were generally closer to the range of relevant natural periods for anchored components in the CRSBF than in the BRBF. The similar peaks in floor spectra magnitude between the two systems at $\frac{1}{4}$ DBE level was attributed to the fact that at median levels the BRBF structures were just barely beginning to yield and therefore were not able to take advantage of the spreading and capping effect on the floor spectra caused by yielding. This is the most important observation in comparing the performance of acceleration-sensitive

nonstructural components between CRSBFs and conventional systems with distributed plasticity, as the trade-off for the intended structural benefit of maintaining elasticity in the frame members, was large, concentrated peaks in floor spectra that were formed due to the frame vibrating in the higher-mode frequencies.

This study also analyzed the performance of two common types of unanchored nonstructural components: sliding and rocking components. The performance of sliding components at DBE level was also generally better in the BRBFs than the CRSBFs, where sliding displacements and velocities were larger in the CRSBFs at most but not all floors. This observation matched up fairly well with the relative differences in peak floor accelerations between the two systems, although at friction coefficients below 0.2, the sliding displacements and velocities were much closer between the two systems. At $\frac{1}{4}$ DBE level, sliding component performance was similar between the two systems, although negligible sliding occurred for components with friction coefficients greater than 0.2. These results were also fairly consistent across all structure heights. In contrast to the performance of anchored components and sliding components, the performance of unanchored rocking components was generally similar between the two systems at DBE level, especially for the two more slender components of $\alpha = 10^\circ$ and $\alpha = 15^\circ$, where performance in the CRSBFs was similar or sometimes even better than that of the BRBFs. The stockiest rocking component with $\alpha = 20^\circ$ experienced better performance in the BRBF, more consistent with the lower values of peak floor accelerations for the BRBF. At the $\frac{1}{4}$ DBE level, the two stockier rocking components experienced negligible rocking response, whereas the $\alpha = 10^\circ$ rocking component did see overturning for some of the smallest sized components.

Some of the driving influences for nonstructural component demands in CRSBFs were also examined. In order to compare the influence that the base rocking moment and supplemental energy dissipation had on the floor spectra, nonlinear-time history analyses were repeated for the two CRSBF base rocking joint designs, which varied in rocking moment and supplemental energy dissipation, using the same frame members for both CRSBFs. The results suggested that the amount of energy dissipation provided in the CRSBF base rocking joint design had a minimal effect on the floor spectra magnitudes, particularly in the higher-mode period range of the CRSBF, and the differences were more influenced by differences in the base rocking moment.

Finally, to investigate any potential effects of the CRSBF grounding on the response of the nonstructural components, the floor accelerations, anchored component pseudo-accelerations, sliding component, and rocking component responses were analyzed. There was no indication that the transition of the system transferring from a low lateral stiffness, during rocking, to a high lateral stiffness, at grounding, led to any spiking effects in the floor accelerations or noticeable changes in the response trend of the nonstructural components. Also explored was whether or not the higher-mode effects, known to increase CRSBF member forces, would also lead to an increase in floor acceleration response. Although it was true that large peaks in floor spectra did occur at the higher-mode rocking periods of the CRSBFs, the concentration and magnitudes of these peaks compared to the BRBF floor spectra suggested that the acceleration response was likely driven by the fact that the CRSBF did not experience member yielding, and therefore was not relieved from

vibrating in its elastic modes during each ground motion, rather than the CRSBFs experiencing a significantly larger participation of higher modes compared to the BRBF.

Overall, the results of this study demonstrated that over a range of varying structure heights, the demands on anchored and unanchored nonstructural components were typically larger in CRSBFs than in a BRBF. This was primarily a consequence of capacity protecting the frame members to remain elastic, rather than a product of abrupt stiffness changes while rocking or significantly larger participation of the higher modes.

7.2 Recommendations

Moving forward, it will be important to determine if nonstructural component demands in the CRSBF system exceed levels deemed acceptable by typical design standards, as large demands on nonstructural components not only threaten the economic viability for using this self-centring system, but can also pose a significant health risk to occupants in the structure. This is particularly the case for anchored components, where significant differences in peak floor spectra magnitudes between the CRSBF and BRBF system may not just be an economic concern for using CRSBFs, but a safety concern. For example, in the case of installing a common suspended ceiling system which has shown adequate seismic performance in structures with conventional seismic force resisting systems with distributed plasticity, the large peaks in CRSBF floor spectra suggest that the suspending ceiling system has the potential to experience demands that are multiple times greater than potentially expected. As the CRSBF system pushes towards becoming a fully codified system in many design standards, the consideration of these large magnitudes in floor spectra is imperative. From an economic point of view, although CRSBFs provide

structural advantages over using a conventional system, if the trade-off for this structural performance is significant losses due to nonstructural component performance, the resiliency and economic viability of using CRSBFs as a high-performance solution may be hindered.

When considering the influence that CRSBF design decisions have on nonstructural component performance, this study showed that the amount of energy dissipation provided in the base rocking joint design had a negligible influence on floor acceleration demands when considering CRSBFs of similar stiffness and rocking moment. However, during the CRSBF design process the amount of energy dissipation did have an impact on the base rocking moment and frame member capacity designs, both of which seem to influence nonstructural component performance. At all building heights, the CRSBFs designed with more energy dissipation were able to meet their target drift performance while having a lower rocking moment, and more flexible frame, which in general resulted in lower demands on acceleration-sensitive anchored components, unanchored sliding components and unanchored rocking components. This result makes sense when considering that seismic hazard, defined by a response spectrum, generally reduces in pseudo-acceleration as the period of a structure gets longer (with the exception of very short periods). Therefore, the recommendation to a CRSBF designer considering the performance of nonstructural components would be: CRSBFs designed with the most flexible frame and lowest rocking moment possible, provided the target interstorey drift performance, frame member capacity design objectives, and collapse performance of the design are still maintained, will generally experience lower demands on nonstructural components; and the best way to

achieve this type of design is with a larger amount of energy dissipation provided in the base rocking joint design. Nevertheless, this design recommendation does not always lead to a significant improvement in nonstructural component performance (as was the case for the 6-storey CRSBFs) and therefore a potential area of future research could be developing mitigation strategies for reducing demands on nonstructural components in CRSBFs while attempting to maintain the structural performance of the system.

Finally, the results of this study leave two important questions and potential areas of future research on the performance of nonstructural components in CRSBFs and their viability as a high-performance seismic design solution: at what point do the demands on nonstructural components in CRSBFs change from simply being an economic consideration to a public safety concern, and what is the cost-benefit or loss estimation comparison of using CRSBFs over conventional seismic force resisting systems with distributed plasticity, accounting for both structural and nonstructural costs?

References

- American Institute of Steel Construction (AISC). [2016] *Specification for Structural Steel Buildings*, ANSI/AISC Standard 360-16, Chicago, IL, USA.
- American Institute of Steel Construction (AISC). [2016] *Seismic Provisions for Structural Steel Buildings*, ANSI/AISC Standard 341-16, Chicago, IL, USA.
- American Society of Civil Engineers (ASCE). [2016] *Minimum Design Loads and Associated Criteria for Buildings and Other Structures*, ASCE/SEI Standard 7-16, Reston, VA, USA.
- Applied Technology Council. [2012] *Reducing the Risks of Nonstructural Earthquake Damage – A Practical Guide*, FEMA Report E-74, Prepared for the Federal Emergency Management Agency, Washington, DC, USA.
- Applied Technology Council. [2009] *Quantification of Building Seismic Performance Factors*, FEMA Report P695, Prepared for the Federal Emergency Management Agency, Washington, DC, USA.
- Buchanan, A.H., Bull, D., Dhakal, R., MacRae, G., Palermo, A., Pampanin, S. [2011] “Base Isolation and Damage-Resistant Technologies for Improved Seismic Performance of Buildings,” *Royal Commission of Inquiry into Building Failure Caused by the Canterbury Earthquakes: Research Report 2011-02*, Department of Civil and Natural Resources Engineering, University of Canterbury, Christchurch, New Zealand.
- Chaudhuri, S.R., Hutchinson, T.C. [2005] “Characterizing frictional behavior for use in predicting the seismic response of unattached equipment,” *Soil Dynamics and Earthquake Engineering*, Vol. 25(7-10), pp. 591-604.
- Chaudhuri, S.R., Hutchinson, T.C. [2006] “Fragility of Bench-Mounted Equipment Considering Uncertain Parameters,” *Journal of Structural Engineering*, Vol. 132(6), pp. 884-898.
- Choi, B., Tung, C.C.D. [2002] “Estimating Sliding Displacement of an Unanchored Body Subjected to Earthquake Excitation,” *Earthquake Spectra*, Vol. 18, No. 4, pp. 601-613.
- Comerio, M.C. [2005] “PEER Testbed Study on a Laboratory Building: Exercising Seismic Performance Assessment,” *Report PEER 2005/12*, Pacific Earthquake Engineering Research Center, University of California, Berkeley, USA.

- Dyanati, M., Huang, Q., Roke, D. [2014] “Structural and Nonstructural Performance Evaluation of Self-Centering Concentrically Braced Frames Under Seismic Loading,” *Proceedings of ASCE 2014 Structures Congress*, Boston, MA, USA.
- Eatherton, M.R., Hajjar, J.F. [2010] “Large-Scale Cyclic and Hybrid Simulation Testing and Development of a Controlled-Rocking Steel Building System with Replaceable Fuses,” *NSEL Report NSEL-025*, Department of Civil and Environmental Engineering, University of Illinois at Urbana-Champaign, USA.
- Eatherton, M.R., Ma, X., Krawinkler, H., Mar, D., Billington, S., Hajjar, J., Deierlein, G. [2014] “Design concepts for controlled rocking of self-centering steel-braced frames,” *Journal of Structural Engineering*, Vol. 140(11), No. 4014082.
- Filiatrault, A., Kuan, S., Tremblay, R. [2004] “Shake table testing of bookcase – partition wall systems,” *Canadian Journal of Civil Engineering*, Vol. 31, No. 4, pp. 664-676.
- Filiatrault, A., Uang, C.-M., Folz, B., Christopoulos, C., Gatto, K. [2001] “Reconnaissance report of the February 28, 2001 Nisqually (Seattle-Olympia) earthquake,” *Report No. SSRP-2001/02 for the Structural Systems Research Project*, University of California, San Diego, La Jolla, USA.
- Gledhill, S.M., Sidwell, G.K., Bell, D.K. [2008] “The Damage Avoidance Design of tall steel frame buildings - Fairlie Terrace Student Accommodation Project, Victoria University of Wellington.,” *Proceedings of the 2008 NZSEE Conference*, Wairakei, New Zealand.
- Housner, G.W. [1963] “The behavior of inverted pendulum structures during earthquakes,” *Bulletin of the Seismological Society of America*, Vol. 53, No. 2, pp. 403-417.
- Hutchinson, T.C., Chaudhuri, S.R. [2006] “Bench–shelf system dynamic characteristics and their effects on equipment and contents,” *Earthquake Engineering & Structural Dynamics*, Vol. 35, No. 13, pp. 1631-1651.
- Kazantzi, A., Vamvatsikos, D., Miranda, E. [2018] “Effect of yielding on the seismic demands of nonstructural elements,” *Proceedings of the 16th European Conference on Earthquake Engineering*, Thessaloniki, Greece.
- Konstantinidis, D., Makris, N. [2009] “Experimental and analytical studies on the response of freestanding laboratory equipment to earthquake shaking,” *Earthquake Engineering & Structural Dynamics*, Vol. 38, No. 6, pp. 827-848.
- Konstantinidis, D., Makris, N. [2010] “Experimental and analytical studies on the response of 1/4-scale models of freestanding laboratory equipment subjected to strong earthquake shaking,” *Bulletin of Earthquake Engineering*, Vol. 8, No. 6, pp. 1457-1477.

- Konstantinidis, D., Nikfar, F. [2015] “Seismic response of sliding equipment and contents in base-isolated buildings subjected to broadband ground motions,” *Earthquake Engineering & Structural Dynamics*, Vol. 44, No. 6, pp. 865-887.
- Kwon, O.-S., Kim, E.S. [2010] “Evaluation of building period formulas for seismic design,” *Earthquake Engineering & Structural Dynamics*, Vol. 39, No. 14, pp. 1569-1583.
- Latham, D.A., Reay, A.M., Pampanin, S. [2013] “Kilmore Street Medical Centre: Application of a Post-Tensioned Steel Rocking System,” *Proceedings of the Steel Innovations Conference 2013*, Christchurch, New Zealand.
- Lin, S.L., MacRae, G.A., Dhakal, R.P., Yeow, T.Z. [2012] “Contents Sliding Response Spectra,” *Proceedings of 15th World Conference on Earthquake Engineering*, Lisboa, Portugal.
- Lin, S.L., MacRae, G.A., Dhakal, R.P., Yeow, T.Z. [2015] “Building contents sliding demands in elastically responding structures,” *Engineering Structures*, Vol. 86, pp. 182-191.
- Linde, S. [2016] “Rocking response of slender freestanding building contents in fixed-based and base-isolated buildings,” *M.A.Sc. Thesis*, McMaster University, Hamilton, Ontario, Canada.
- Lopez Garcia, D., Soong, T.T. [2003a] “Sliding fragility of block-type non-structural components. Part 1: unrestrained components,” *Earthquake Engineering & Structural Dynamics*, Vol. 32, No. 1, pp. 111-129. MATLAB. [2017] Version 2017b, *The Language of Technical Computing*, The Mathworks, Inc.: Natick, USA.
- Ma, X., Krawinkler, H., Deierlein, G. [2010] “Seismic Design and Behavior of Self-Centering Braced Frame with Controlled Rocking and Energy-Dissipating Fuses,” *Blume Earthquake Engineering Center Report 174*, Department of Civil and Environmental Engineering, Stanford University, USA.
- Makris, N., Konstantinidis, D. [2003] “The rocking spectrum and the limitations of practical design methodologies,” *Earthquake Engineering & Structural Dynamics*, Vol. 32, No. 2, pp. 265-289.
- Makris, N., Roussos, Y.S. [1998] “Rocking response and overturning of equipment under horizontal pulse-type motions,” *Report PEER 1998/05*, Pacific Earthquake Engineering Research Center, University of California, Berkeley, USA.
- Makris, N., Roussos, Y.S. [2000] “Rocking response of rigid blocks under near-source ground motions,” *Géotechnique*, Vol. 50, No. 3, pp. 243-262.

- McCormick, J., Aburano, H., Ikenaga, M., Nakashima, M. [2008] “Permissible residual deformation levels for building structures considering both safety and human elements,” *Proceedings of 14th World Conference on Earthquake Engineering*, Beijing, China.
- Miranda, E., Mosqueda, G., Retamales, R., Pekcan, G. [2012] “Performance of non-structural components during the 27 February 2010 Chile earthquake,” *Earthquake Spectra*, Vol. 28, No. S1, pp. S453-S471.
- Mottier, P., Tremblay, R., Rogers, C. [2018] “Seismic retrofit of low-rise steel buildings in Canada using rocking steel braced frames,” *Earthquake Engineering & Structural Dynamics*, Vol. 47, No. 2, pp. 333-355.
- Nikfar, F., N.A., Konstantinidis, D. [2017] “Effect of the Stick-Slip Phenomenon on the Sliding Response of Objects Subjected to Pulse Excitation,” *Journal of Engineering Mechanics*, Vol. 143(4), No. 04016122.
- Pacific Earthquake Engineering Research Center (PEER). [2015] Open System for Earthquake Engineering Simulation v2.4.4, [Computer Software].
- Pollino, M. [2014] “Seismic design for enhanced building performance using rocking steel braced frames,” *Engineering Structures*, Vol. 83, pp. 129-139.
- Priestley, M.J.N., Calvi, G.M., Kowalsky, M.J. [2007] “Displacement-based seismic design of structures,” *IUSS Press*, Pavia, Italy.
- Roke, D., Sause, R., Ricles, J.M., Chancellor, N.B. [2010] “Damage-Free Seismic-Resistant Self-Centering Concentrically-Braced Frames,” *ATLSS Report 10-09*, Lehigh University, USA.
- Saxey, B., Daniels, M. [2014] “Characterization of overstrength factors for buckling restrained braces,” *Proceedings of Australasian Structural Engineering Conference*, Auckland, New Zealand.
- Shao, Y., Tung, C.C.D. [1999] “Seismic Response of Unanchored Bodies,” *Earthquake Spectra*, Vol. 15, No. 3, pp. 523-536.
- Shenton, H.W. [1996] “Criteria for Initiation of Slide, Rock, and Slide-Rock Rigid-Body Modes,” *Journal of Engineering Mechanics*, Vol. 122, No. 7, pp. 690-693.
- Steele, T.C. [2019] “Ultimate limit states in Controlled Rocking Steel Braced Frames,” *Ph.D. Thesis*, McMaster University, Hamilton, Ontario, Canada.
- Steele, T.C., Wiebe, L. [2016] “Dynamic and equivalent static procedures for capacity design of controlled rocking steel braced frames,” *Earthquake Engineering & Structural Dynamics*, Vol. 45, No. 14, pp. 2349-2369.

- Steele, T.C., Wiebe, L. [2017] “Collapse risk of controlled rocking steel braced frames with different post-tensioning and energy dissipation designs,” *Earthquake Engineering & Structural Dynamics*, Vol. 46, No. 13, pp. 2063-2082.
- Taghavi, S., Miranda, E. [2003] “Response Assessment of Nonstructural Building Elements,” *Report PEER 2003/05*, Pacific Earthquake Engineering Research Center, University of California, Berkeley, USA.
- Van Engelen, N., Konstantinidis, D., Tait, M. [2016] “Structural and nonstructural performance of a seismically isolated building using stable unbonded fiber-reinforced elastomeric isolators,” *Earthquake Engineering & Structural Dynamics*, Vol. 45, No. 3, pp. 421-439.
- Wiebe, L., Christopoulos, C. [2010] “Characterizing acceleration spikes due to stiffness changes in nonlinear systems,” *Earthquake Engineering & Structural Dynamics*, Vol. 39, pp. 1653-1670.
- Wiebe, L., Christopoulos, C., Tremblay, R., Leclerc, M. [2013] “Mechanisms to limit higher mode effects in a controlled rocking steel frame. 2: Large-amplitude shake table testing,” *Earthquake Engineering & Structural Dynamics*, Vol. 42, pp. 1069-1086.
- Wiebe, L., Christopoulos, C. [2015a] “Performance-Based Seismic Design of Controlled Rocking Steel Braced Frames. I: Methodological Framework and Design of Base Rocking Joint,” *Journal of Structural Engineering*, Vol. 141(9), No. 04014226.
- Wiebe, L., Christopoulos, C. [2015b] “Performance-Based Seismic Design of Controlled Rocking Steel Braced Frames. II: Design of Capacity-Protected Elements,” *Journal of Structural Engineering*, Vol. 141(9), No. 04014227.
- Yim, C.-K., Chopra, A., Penzien, J. [1980] “Rocking response of rigid blocks to earthquakes,” *Report No. UCB/EERC-80/02*, Earthquake Engineering Research Center, University of California, Berkeley, USA.
- Zhang, C., Steele, T.C., Wiebe, L. [2018] “Design-level estimation of seismic displacements for self-centering SDOF systems on stiff soil,” *Engineering Structures*; Vol. 177, pp. 431-443.

Appendix A: Final Design Frame Sections

Table A.1 3S- β 25 CRSBF frame members

Storey	Brace	Column	Beam
1	W310x283	W310x500	W200x86
2	W310x179	W310x500	W310x226
3	W310x500	W310x500	W200x42

Table A.2 3S- β 90 CRSBF frame members

Storey	Brace	Column	Beam
1	W310x179	W310x283	W200x52
2	W250x131	W310x283	W250x131
3	W310x283	W310x283	W200x42

Table A.3 3S BRBF frame members

Storey	BRB Core Area (mm ²)	Column	Beam
1	4597	W250x89	-
2	3710	W250x89	-
3	1855	W250x89	-

Table A.4 6S- β 25 CRSBF frame members

Storey	Brace	Column	Beam
1	W310x202	W360x509	W200x71
2	W250x167	W360x509	W200x52
3	W250x115	W310x500	W200x52
4	W250x131	W310x500	W200x59
5	W250x131	W310x313	W310x202
6	W310x415	W310x313	W200x42

Table A.5 6S- β 90 CRSBF frame members

Storey	Brace	Column	Beam
1	W250x167	W310x342	W200x52
2	W250x131	W310x342	W200x42
3	W200x100	W310x313	W200x42
4	W250x101	W310x313	W200x46
5	W250x115	W310x179	W250x115
6	W310x226	W310x179	W200x42

Table A.6 6S BRBF frame members

Storey	BRB Core Area (mm ²)	Column	Beam
1	6129	W360x196	-
2	5806	W360x196	-
3	5323	W310x117	-
4	4516	W310x117	-
5	3226	W200x52	-
6	1694	W200x52	-

Table A.7 12S-β25 CRSBF frame members

Storey	Brace	Column	Beam
1	W310x313	W360x900	W250x149
2	W310x283	W360x900	W250x115
3	W310x253	W360x900	W200x100
4	W310x202	W360x900	W200x86
5	W310x158	W360x900	W200x71
6	W250x167	W360x900	W200x86
7	W310x179	W360x818	W200x86
8	W310x202	W360x818	W200x100
9	W310x202	W360x744	W200x86
10	W310x179	W360x744	W200x71
11	W250x167	W360x592	W200x42
12	W250x89	W360x592	W200x42

Table A.8 12S-β90 CRSBF frame members

Storey	Brace	Column	Beam
1	W310x283	W360x551	W250x115
2	W310x253	W360x551	W200x100
3	W310x202	W360x634	W200x86
4	W310x158	W360x634	W200x59
5	W250x149	W360x634	W200x59
6	W250x131	W360x634	W200x71
7	W250x167	W360x592	W200x86
8	W310x158	W360x592	W200x86
9	W310x179	W360x509	W200x86
10	W310x158	W360x509	W200x59
11	W250x149	W310x415	W200x42
12	W200x100	W310x415	W200x42

Table A.9 12S BRBF frame members

Storey	BRB Core Area (mm ²)	Column	Beam
1	8387	W360x551	-
2	8226	W360x551	-
3	8226	W360x421	-
4	8065	W360x421	-
5	7903	W360x314	-
6	7419	W360x314	-
7	6935	W360x196	-
8	6290	W360x196	-
9	5323	W310x117	-
10	4194	W310x117	-
11	3145	W200x52	-
12	1694	W200x52	-

Appendix B: Floor Spectra with Extended Period Range

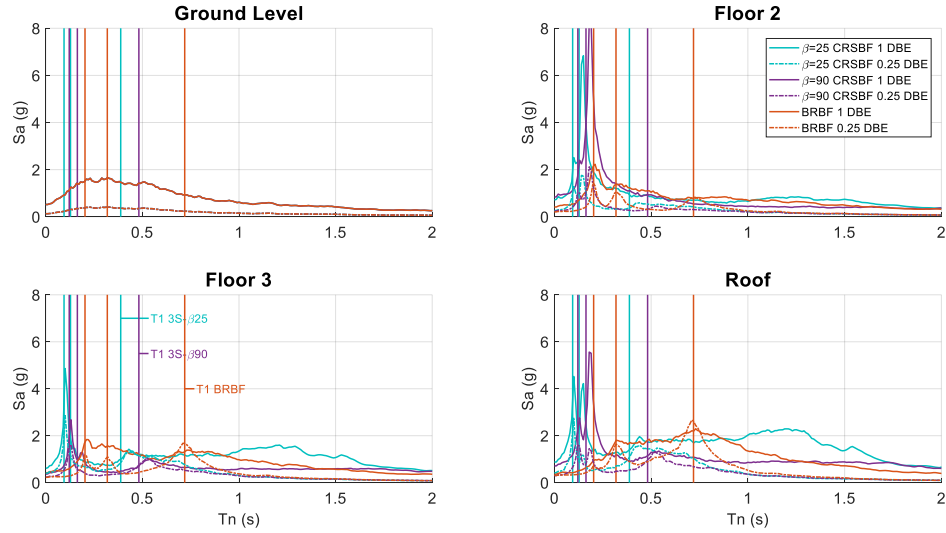


Figure B.1 3-storey CRSBF and BRBF median pseudo-acceleration floor spectra with $\zeta=2\%$ and extended period range

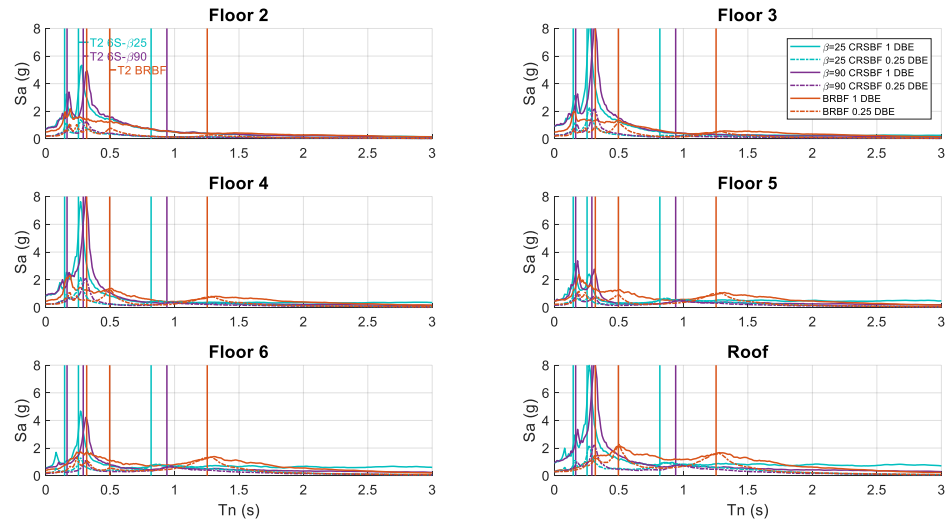


Figure B.2 6-storey CRSBF and BRBF median pseudo-acceleration floor spectra with $\zeta=2\%$ and extended period range

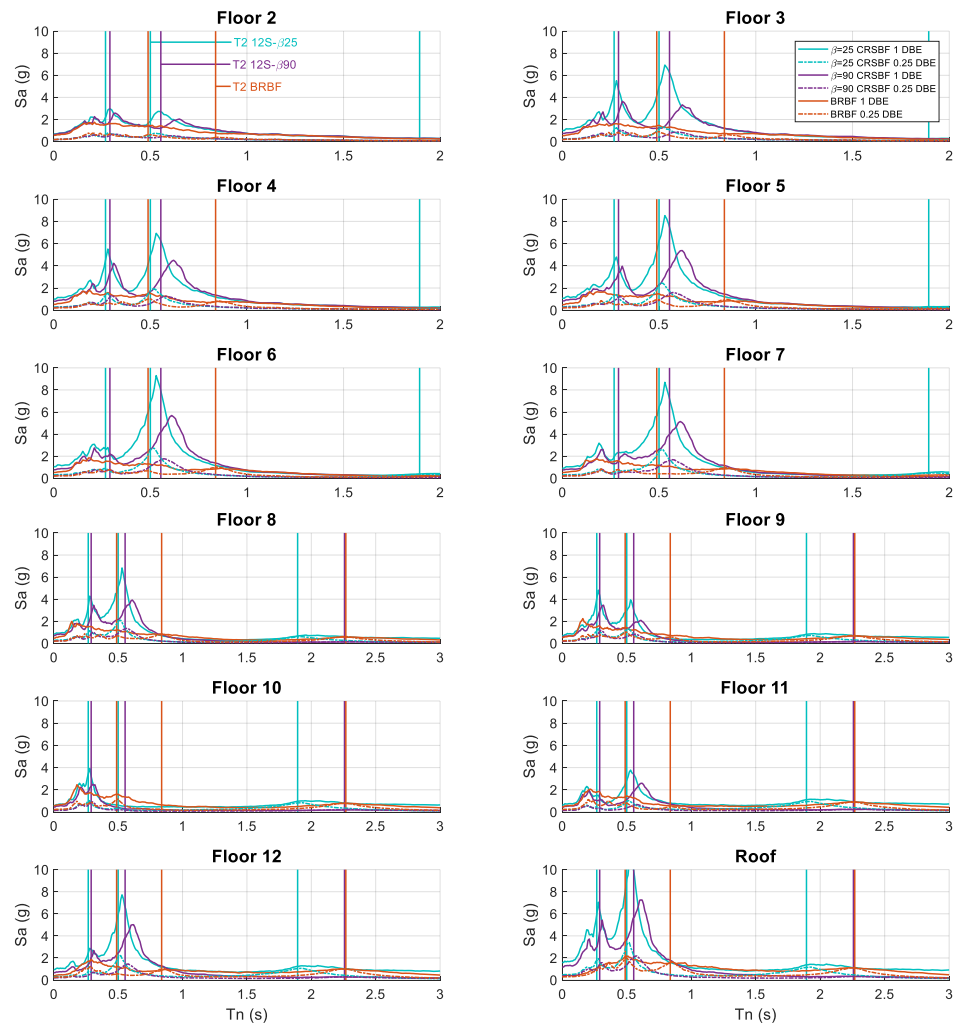


Figure B.3 12-storey CRSBF and BRBF median pseudo-acceleration floor spectra with $\zeta=2\%$ and extended period range

Appendix C: CRSBF Floor Spectra with Identical Frames and Extended Period Range

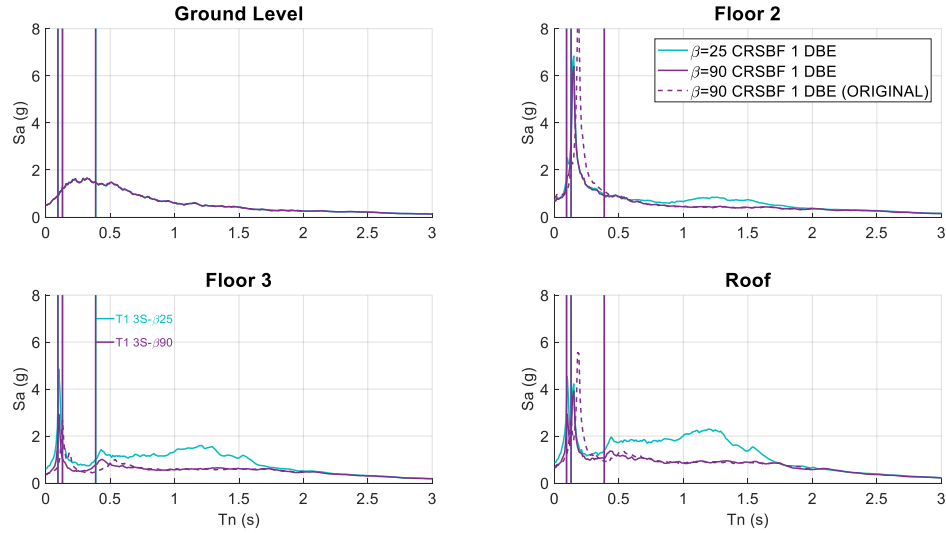


Figure C.1 3-storey CRSBFs designed with identical frames, median pseudo-acceleration floor spectra with $\zeta = 2\%$ with extended period range

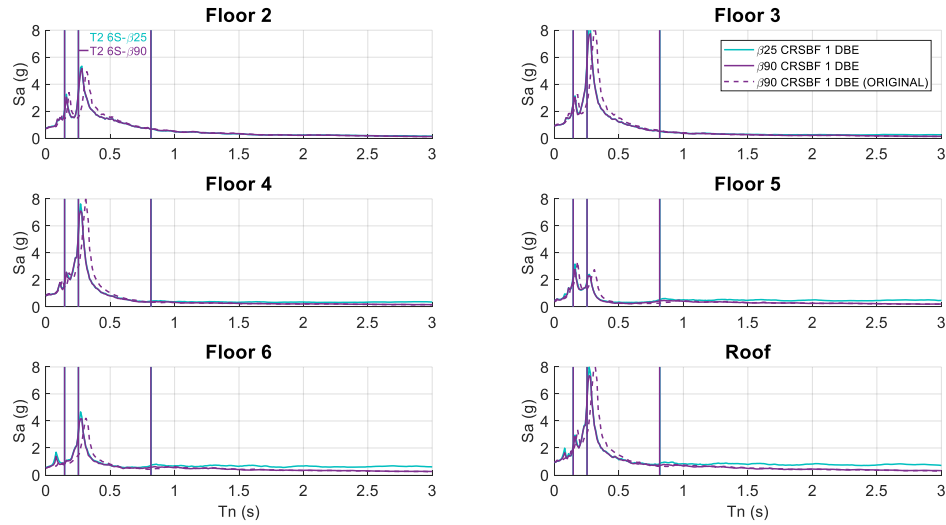


Figure C.2 6-storey CRSBFs designed with identical frames, median pseudo-acceleration floor spectra with $\zeta = 2\%$ with extended period range

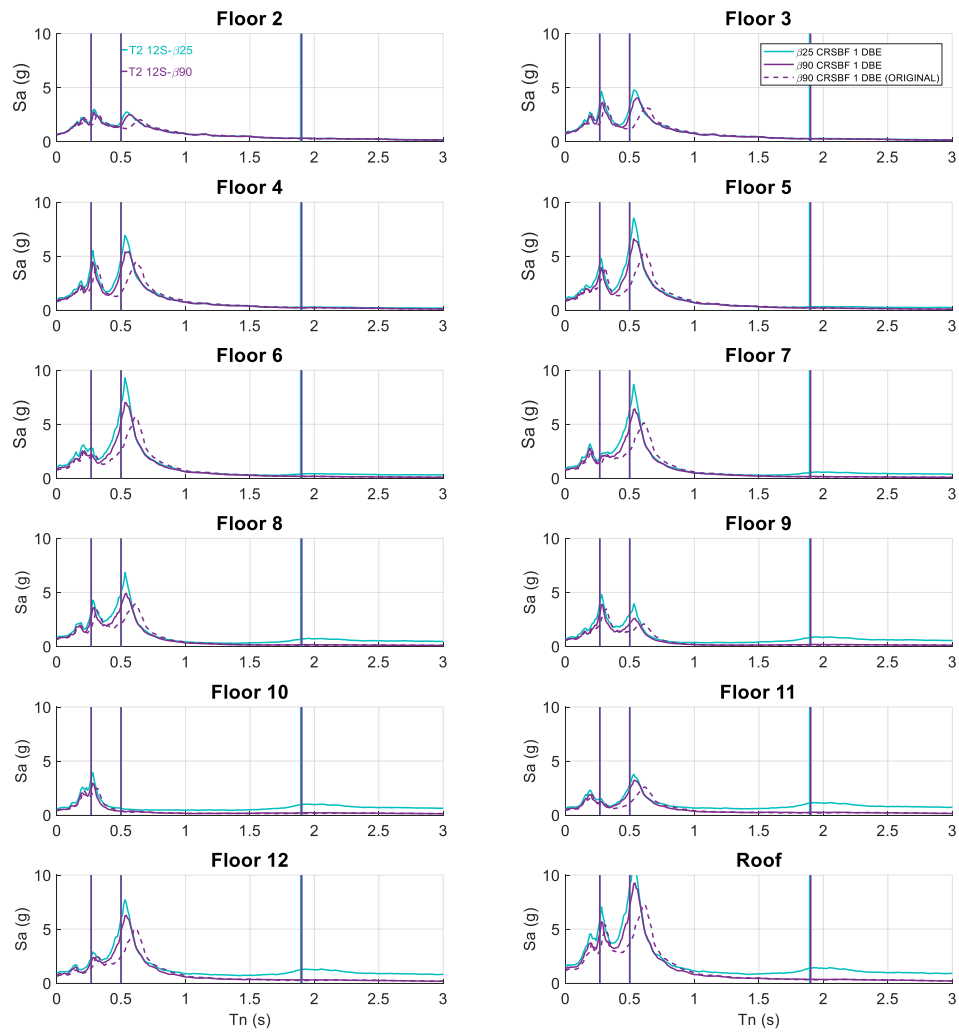


Figure C.3 12-storey CRSBFs designed with identical frames, median pseudo-acceleration floor spectra with $\zeta = 2\%$ with extended period range